SANTIAGO VIANNA CUADRA

DESENVOLVIMENTO DE UM MODELO BIOFÍSICO DE CRESCIMENTO DA CANA-DE-AÇÚCAR PARA ESTUDOS GLOBAIS

Tese apresentada à Universidade Federal de Viçosa, como parte das exigências do Programa de Pós-Graduação em Meteorologia Agrícola, para obtenção do título de *Doctor Scientiae*.

VIÇOSA
MINAS GERAIS – BRASIL
2010

Ficha catalográfica preparada pela Seção de Catalogação e Classificação da Biblioteca Central da UFV

T
C961d
2010

Cuadra, Santiago Vianna, 1976-
Desenvolvimento de um modelo biofísico de crescimento da cana-de-açúcar para estudos globais / Santiago Vianna Cuadra. – Viçosa, MG, 2010.
xii, 68f. : il. (algumas col.) ; 29cm.

Orientador: Marcos Heil Costa.
Tese (doutorado) - Universidade Federal de Viçosa.
Referências bibliográficas: f. 59-68

1. Meteorologia agrícola. 2. Climatologia agrícola - Modelos matemáticos. 3. Cana-de-açúcar.
4. Biocombustíveis. I. Universidade Federal de Viçosa. II. Título.

CDD 22. ed. 630.2515

SANTIAGO VIANNA CUADRA

DESENVOLVIMENTO DE UM MODELO BIOFÍSICO DE CRESCIMENTO DA CANA-DE-AÇÚCAR PARA ESTUDOS GLOBAIS

Tese apresentada à Universidade Federal de Viçosa, como parte das exigências do Programa de Pós-Graduação em Meteorologia Agrícola, para obtenção do título de *Doctor Scientiae*.

APROVADA: 26 de novembro de 2010.

Edson Luís Nunes

Paulo José Hamakawa

José Maria Nogueira da Costa

José Maria Nogueira da Costa

Rosmeri Porfírio da Rocha
(Coorientadora)

Marcos Heil Costa
(Orientador)

A Deus, pela vida e pelo amor.
À minha esposa Ana Paula Gomes Cuzziol
e à minha filha Maria Luiza Cuzziol Cuadra.
À minha mãe Denise Vianna e ao meu pai José Lopez.
À minha sogra Virgínia Maria Gomes Carllini.
Aos meus irmãos Carina, Ítalo, Pablo, José Luiz e Soledad.

AGRADECIMENTOS

À Universidade Federal de Viçosa e ao Departamento de Engenharia Agrícola, pela oportunidade de realização do curso.

À CAPES, pela concessão da bolsa de estudos.

BIOGRAFIA

SANTIAGO VIANNA CUADRA, filho de José Lopez e Denise Vianna, nasceu em 15 de dezembro de 1976 no Rio de Janeiro, RJ.

SUMÁRIO

LISTA DE ABREVIATURAS

APAR – Absorbed Photosynthetic Active Radiation.
DAR – Days After Ratooning.
GCM – Global Climate Model.
GDD – Growing Degree Days.
IBGE – Brazilian Institute of Geography and Statistics.
IBIS – Integrated Biosphere Simulator.
LAI – Leaf Area Index.
LSM – Land Surface Models.
NEE – Net Ecosystem Exchange.
NPP – Net Primary Production.
PFT – Plant Functional Type.
RMSE – Root Mean Square Error.
RUE – Radiation Use Efficiency.
SLA – Specific Leaf Area.

LISTA DE SÍMBOLOS

Ag – Gross photosynthesis rate.

AR_s – Absorbed solar radiation.

β – Bowen ratio.

ET – Evapotranspiration.

ET_0 – Reference evapotranspiration.

FRW – Furrow irrigated.

G – Soil heat flux.

H – Relative humidity.

H – Sensible heat flux.

K_e – Radiation extinction coefficient.

λE – Latent heat flux.

RM – Crop relative maturity.

R_n – Net radiation.

R_p – Photosynthetic active radiation flux.

R_s – Solar radiation flux.

V_{max} – Maximum capacity of rubisco enzyme.

χ_L – Leaf angle departure.

RESUMO

CUADRA, Santiago Vianna, D.Sc., Universidade Federal de Viçosa, novembro de 2010. **Desenvolvimento de um modelo biofísico de crescimento da cana-de-açúcar para estudos globais**. Orientador: Marcos Heil Costa. Coorientadores: Aristides Ribeiro e Rosmeri Porfírio da Rocha.

Previsões apontam uma expansão das terras cultivadas ao longo das próximas décadas devido a uma combinação do aumento da população global, com consequente necessidade de aumento da produção de alimentos, e do recente crescimento exponencial da produção de biocombustíveis baseados em cultura agrícolas. As alterações resultantes do uso da terra podem, por sua vez, impactar significativamente os ciclos biogeoquímicos e biogeofísicos ao longo do globo. Portanto, a representação de culturas agrícolas para produção de biocombustíveis, como a cana-de-açúcar, devem ser integradas em modelos de processos superficiais terrestres, possibilitando considerar nas simulações numéricas os *feedbacks* bidirecionais entre a superfície e a atmosfera. Neste estudo, nós apresentamos um novo modelo mecanicista de crescimento da cultura da cana-de-açúcar, incluído como um módulo dentro do modelo dinâmico de agro-ecossistema Agro-IBIS, que pode ser aplicado em múltiplas escalas espaciais (do local ao global). O modelo pode ser acoplado a um modelo atmosférico, permitindo a simulação das interações bidirecionais entre a atmosfera e o sistema de cultivo de cana. Esse novo módulo inclui uma série de equações e parâmetros de manejo agrícola que diferem das formulações para as culturas anuais pré-existentes. O modelo é avaliado contra observações micro-meteorológicas e de biomassa, obtidas para um ciclo da cultura (391 dias), no norte do Estado de São Paulo (Brasil), e para a produtividade agrícola em diferentes escalas espaciais. Os resultados da validação micro-meteorológica indicam que o modelo produz robustamente as flutuações sazonais e diárias do albedo, biomassa seca, e as relações entre troca líquida do ecossistema (NEE) e das variáveis atmosféricas (temperatura e umidade relativa do ar). Ao nível local, o modelo simulou com precisão a intensidade e a variabilidade diária da evapotranspiração (ET) durante dois ciclos consecutivos da cana-de-açúcar em um sítio experimental na localidade Kalamia, nordeste da Austrália. O modelo simulou com exatidão a média da produtividade da cana-de-açúcar para as quatro maiores mesorregiões produtoras (aglomerados de municípios) do estado de São Paulo (Brasil), durante um período de 16 anos, com viés relativo entre -0,68% e +1,08%. Finalmente, a simulação da produtividade média anual de cana para o Estado de Louisiana (EUA) produziu um viés relativo (-2,67%) baixo, mas apresentou menor variabilidade interanual do que a série de produtividade estimada. Considerando os resultados de todas as validações, podemos concluir que o novo modelo é capaz de capturar a relação entre a produção de biomassa e variabilidade do clima (temperatura e precipitação), indicando que o módulo pode ser utilizado com sucesso para prever alterações nos sistemas de cultivo de cana e as respectivas interações com o clima.

ABSTRACT

CUADRA, Santiago Vianna, D.Sc., Universidade Federal de Viçosa, November, 2010. **A biophysical sugarcane growth model for global studies**. Adviser: Marcos Heil Costa. Co-advisers: Aristides Ribeiro and Rosmeri Porfírio da Rocha.

Global agricultural lands are predicted to expand over the next few decades due to a combination of increasing global population, the need for increased food production, and exponential growth in crop-based biofuels production. The resultant changes in land use could, in turn, greatly impact biogeochemical and biogeophysical cycles across the globe. Therefore, representation of biofuel crops such as sugarcane should be integrated into the latest models to ensure that accurate simulations of the bidirectional feedbacks between the land surface and atmosphere take place. In this study, we present a new process-based sugarcane model, included as a module within the Agro-IBIS dynamic agro-ecosystem model, that can be applied at multiple spatial scales (from site to global). The model may be coupled to an atmospheric model, allowing the simulation of the bi-directional interactions between atmosphere and the sugarcane cropping system. It includes a series of equations and crop management parameters that differ from the standard formulations for annual crops. The model is evaluated against micro-meteorological and biomass observations, obtained for one crop cycle (391 days) in northern São Paulo state (Brazil), and yield at a range of spatial scales. The results of the micro-meteorological validation suggest that the model produces robust simulations of seasonal and daily albedo fluctuations, dry biomass, and relationships between net ecosystem exchange (NEE) and atmospheric variables (temperature and relative humidity). At the site level, the model accurately simulated the intensity and variability of daily evapotranspiration (ET) for two consecutive crop cycles at an experimental site at Kalamia estate, northeast Australia. The model also accurately simulated the average yield for the four largest mesoregions (clusters of municipalities) in the state of São Paulo (Brazil), over a period of 16 years, with a relative bias of -0.68% to 1.08%. Finally, a simulation of the annual average sugarcane yield over 31 years for the State of Louisiana (U.S.) produced a low relative bias (-2.67%) but exhibited lower yiled interannual variability than the estimated yields. Considering the results of all validations, we conclude that the new model is able to accurately capture the relationship between yield and climate variability (temperature and precipitation), indicating that the module may be successfully used to forecast changes in sugarcane cropping systems and associated climate interactions.

1. INTRODUCTION

The environmental and social impacts of global climate change are one of the greatest challenges facing the human race. Anthropogenic greenhouse gas emissions and land use change (FORSTER et al., 2007; HOUGHTON, 2007; RAMANKUTTY et al., 2008; RAUPACH et al., 2007) are projected to alter the global climate in the next decades (MEEHL et al., 2007). For example, global temperature, precipitation intensity, number of dry days and heat waves are projected to increase and frost days are projected to decrease as result of anthropogenic activities (MEEHL et al., 2007). These changes are expected to have a large impact on both natural and agricultural ecosystems (e.g., COSTA; FOLEY, 2000; MILES et al., 2004; WANG, 2005).

Accordingly to Ramankutty et al. (2008), in the year 2000 cropland covered 15.1 million km^2 while pastureland covered 28.3 million km^2, representing a combined total of about 30% of the global land surface. This significant area of agricultural land is likely to considerably increase in the following decades (FOOD AND AGRICULTURE ORGANIZATION OF THE UNITED NATIONS – FAO, 2008; INTERNATIONAL ENERGY AGENCY – IEA, 2007) under the pressure of an increasing global population, the associated need for increased food production, and the recent expansion of crop-based biofuels production (e.g., ORGANIZATION FOR ECONOMIC CO-OPERATION AND DEVELOPMENT/FOOD AND AGRICULTURE ORGANIZATION OF THE UNITED NATIONS – OECD-FAO, 2007). These land use changes have the potential to greatly influence biogeochemical and biogeophysical processes across the world (e.g., BETTS et al., 2007; COSTA; FOLEY, 2000; HOUGHTON, 2007; PIELKE et al., 1998).

Many studies have highlighted the potential impact of climate change on agriculture and food security (e.g., CHALLINOR et al., 2007; HAIM et al., 2008; TUBIELLO et al., 2007), particularly in developing regions (EASTERLING et al., 2007). Currently, the most frequently used approach to evaluate these impacts is to use crop models that are then forced by the data from Global Climate Model (GCM) projections. However, this approach suffers from a number of inherent limitations. First, most current global climate models work on a scale of tens to hundreds of kilometers (RANDALL et al., 2007), while crop models are usually developed and validated at the site scale (e.g., DUBROVSKY et al., 2000b). Such spatial scale issues are often not considered (e.g., ALEXANDROV; HOOGENBOOM, 2000) or a statistical or dynamical downscaling technique is applied to bridge this difference (e.g., MEARNS et al., 2001).

Another frequently overlooked issue is the fact that crop development is affected not only by the mean atmospheric conditions, but also by the frequency of extreme events such as frost, heat waves, floods, and droughts (e.g., BAIGORRIA et al., 2007; DUBROVSKY et al., 2000a). Many studies have only included mean climatic changes (usually only temperature and precipitation), and considered the present observed climatic variables statistical distribution (e.g., ALEXANDROV; HOOGENBOOM, 2000; FELKNER et al., 2009). In a few cases this limitation was addressed through a stochastic weather generator with modified parameters based on GCMs simulations (e.g., DUBROVSKY et al., 2000b; HAIM et al., 2008).

Another frequently overlooked factor is the bi-directional interaction between land use and climate. Specifically, agriculture may significantly alter atmospheric conditions, particularly over heavily cultivated regions where most of these studies are focused (e.g., BETTS, 2005; COSTA et al., 2007; FEDDEMA et al., 2005; RADDATZ, 2007; TSVETSINSKAYA et al., 2001). Thus, by exclusively focusing on the unidirectional impact of climate change on cropping systems these important feedbacks are not considered.

Land use change can influence the global climate in at least two ways: Firstly, through alterations in biogeochemical processes – usually releasing CO_2 and reducing the capacity of the ecosystem to absorb part of anthropogenic emitted CO_2 (HOUGHTON; HACKLER, 2002; HOUGHTON, 2007). Secondly, by changing the physical properties of the land surface (e.g., BETTS et al., 2007; COSTA; FOLEY, 2000; COSTA; YANAGI, 2006; SNYDER; FOLEY, 2004) thereby altering the energy, mass and momentum balances at surface (PIELKE et al., 1998). For example, the replacement of natural forest by grassland or cropland usually alters the latent and sensible heat fluxes at the surface due to the biophysical differences that characterize these vegetation types – e.g. leaf area index, phenology, stomatal conductance, and root profile (LIU, 2003; SOUZA-FILHO et al., 2005; JUAREZ et al., 2007; TWINE et al., 2004).

Most published studies on the biogeophysical impacts of land use change on climate and ecosystems have focused on the replacement of natural vegetation by pasture land (e.g., COE et al., 2009; COSTA; FOLEY, 2000; NOBRE et al., 1991). However, the biophysical differences between pasture and cropland may result in significantly different interactions with the atmosphere (COSTA et al., 2007). For example, crops usually show a higher seasonal variation in land cover faction (e.g. fallow soil period) and in canopy structure (e.g. leaf area index) than pasture, reflected in more pronounced energy and water surface balance differences across the year as compared to the original forest cover.

Although the models used to predict climate change are improving rapidly (RANDALL et al., 2007), there are still some important processes that have not been incorporated or which are generically characterized. One example is the bi-directional feedbacks between croplands and climate (BETTS, 2005). Crops are not explicitly included in most current land surface schemes coupled to atmospheric models (MEEHL et al., 2007). Furthermore, studies of climate change impacts on crop yield have generally neglected issues of spatial scale, or the impact of extreme weather events on crop yield. These limitations may be largely overcome if crops are explicitly included as part of land surface models (hereinafter referred as Agro-LSMs) and directly coupled to climate models.

Recently, there has been an increasing effort to explicitly represent crops in LSMs (e.g. BONDEAU et al., 2007; GERVOIS et al., 2004; KOTHAVALA et al., 2005; KUCHARIK; BRYE, 2003; LOKUPITIYA et al., 2009; OSBORNE et al., 2007). Diverse approaches have been used to incorporate different crop types within LSMs – with crop types varying from a single generic variety (e.g., OLESON et al., 2007) to thirteen crop classes (BONDEAU et al. 2007). The inherent scale flexibility of Agro-LSMs has lead to their successful application at a range of spatial scales: (i) site level (e.g., BONDEAU et al. 2007; GERVOIS et al., 2004; KOTHAVALA et al., 2005; KUCHARIK AND TWINE, 2007; LOKUPITIYA et al., 2009); (ii) regional level (e.g., KUCHARIK, 2003); (iii) global scale (e.g., BONDEAU et al. 2007; OSBORNE et al., 2007).

Representation of crop growth vary between Agro-LSMs, spanning from: (i) few crop characteristics specifications, (ii) coupling LSM and crop models; and (iii) explicit inclusion of crop growth as function of net crop carbon balance. For example, the Canadian LSM (CLASS) pre-specifies the above ground biomass and empirically calculates LAI based on growing degree days (GDD) and longitude (KOTHAVALA et al., 2005). Gervois et al. (2004) coupled the LSM ORCHIDEE (Organizing Carbon and Hydrology in Dynamic Ecosystems) with the crop model STICS (*Simulateur Multidisciplinaire pour les Cultures Standard*) – and both models are run synchronically and forced with the same atmospheric conditions, and STICS updates ORCHIDEE with LAI, root density profile, nitrogen stress, and vegetation height. In another example, Osborne et al. (2007) incorporated some of the crop model GLAM (General Large-Area Model for annual crops) functions within the LSM MOSES (Met Office Surface Exchange Scheme). Finally, Agro-IBIS (KUCHARIK, 2003), SiBcrop (LOKUPITIYA et al., 2009) and Agro-BGC (DI VITTORIO et al., 2010) incorporates crops phenologic and physiologic characteristics based on previous crop models and literature review. In such approach, crop growth is dependent on net carbon balance – the same vegetation growth principles applied to the natural ecosystems.

However, achieving this objective is not straightforward mainly due to the difficulties to characterize one cropping system at a global scale. Crop management can significantly vary from region to region and crop hybrids may present significant biophysical variations (e.g., EDMÉ et al., 2005; TEJERA et al., 2007). For example, in North America maize has only one crop cycle per year (and may be rotated with typical winter crop such as winter wheat) while in Brazil the common practice is to reap two maize crops per year, in some cases sharing the land with a third crop during the year. This difference determines, for instance, the sowing dates, which is a critical parameter to adequately simulate crop development and its interaction with atmosphere. For regions with marked climatic restrictions on crop growth (e.g., low winter temperatures or a marked dry season) climatic conditions may be a good proxy for sowing dates. However, these are frequently hard to accurately predict as they vary with climatic conditions, biophysical/physiological crop characteristics and management or technological level (e.g., SACKS et al., 2010). Sowing and harvest dates may therefore have a large degree of variability and independence from climatic conditions even in the same region (illustrated in Figure 1). Thus, the derivation of observed global data sets and the simulation of management practices is one of the main challenges when running Agro-LSMs on the global scale (OSBORNE et al., 2007).

Another important challenge in creating a realistic Agro-LSM is how to control the climate model biases when the models are coupled. For instance, at a regional scale climate models may deviate significantly from observations (e.g., DAI, 2006) and affect crop yield. Therefore, climate model biases need to be interactively corrected or considered when crop yield is directly assessed from Agro-LSM coupled simulations (OSBORNE et al., 2007).

Even though atmospheric model bias and crop management practices may have a significant impact on coupled Agro-LSM crop yield simulations (e.g., BAIGORRIA et al., 2007; CHALLINOR et al., 2005; KUCHARIK, 2008), both of these effects can be partially controlled through the off-line application of Agro-LSMs (e.g., GERVOIS et al., 2004; KUCHARIK, 2003; KUCHARIK; TWINE, 2007; OSBORNE et al., 2007). This works in a similar way to off-line uses of crop models (BAIGORRIA et al., 2007; SHIN et al., 2009), whereby an intermediary methodology may be used to correct climate model bias or to incorporate local management practices and hybrid characteristics for local yield assessments.

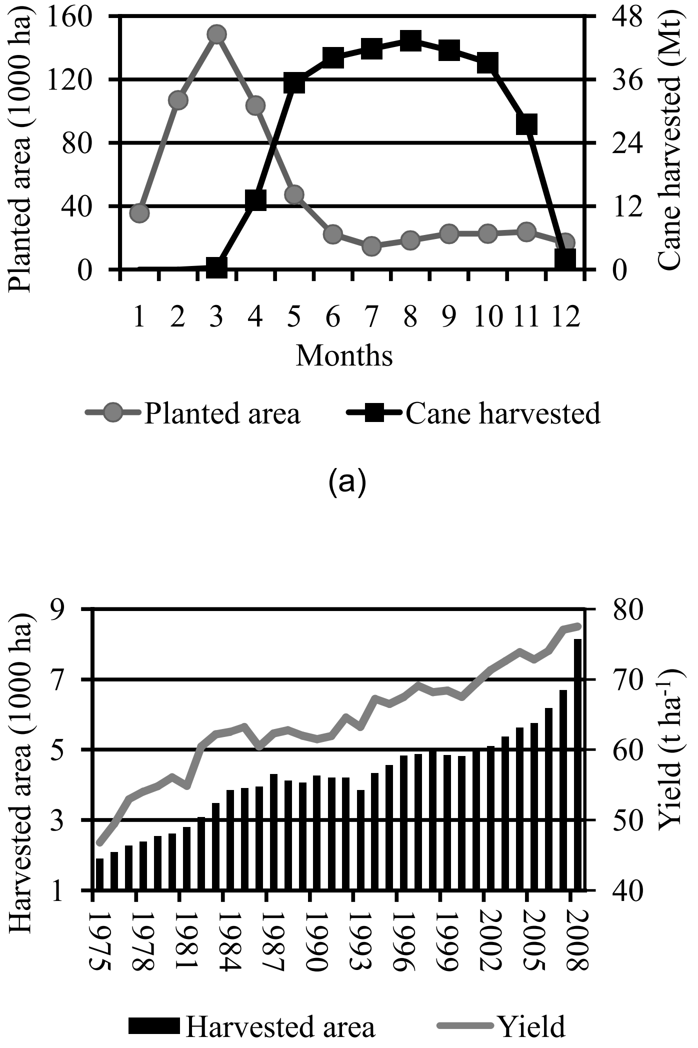

(a)

(b)

Source: Based on IBGE statistics (see text).

Figure 1 – São Paulo state (Brazil) monthly sugarcane planted area (thousands of hectares – k ha) and harvested cane (millions of tons – Mt) for the 2007-08 crop season (a); Brazilian sugarcane harvest area (millions of hectares) and average yield (t ha^{-1}) (b).

The potential of Agro-LSMs to provide more realistic simulations of yield and to simulate land use or management impacts on local to regional climate has led to increasing efforts to explicitly represent different crops in LSMs (e.g., BONDEAU et al., 2007; GERVIOS et al., 2004; KOTHAVALA et al., 2005; KUCHARIK; BRYE, 2003; LOKUPITIYA et al., 2009; OSBORNE et al., 2007). However, as of yet there is no explicit global model of sugarcane growth, phenology, and yield. Sugarcane is becoming increasingly important in the tropics where it is one of the main biofuel crops, beside its use for sugar production. For example, in Brazil sugarcane harvested area increased fourfold from 1975 to 2008 (Figure 1b), while the annual average yield nearly doubled over the same period. In 2007, Brazil sugarcane cultivation accounted for approximately 34% of the 20 millions of hectares that is planted annually across the globe (OECD-FAO, 2007). Additionally, among crops used for biofuel production, sugarcane is an energy crop with one of the highest rates of renewable energy output (MACEDO, 2006) and biofuel yields per area (GIBBS et al., 2008). Moreover, it has one of the lowest biofuel production costs (US$ per liter; OECD-FAO, 2008) and ecosystem ‘carbon payback times’ (FARGIONE et al., 2008; GIBBS et al., 2008). It has thus become one of the most important global crops for renewable energy production, carbon savings, land use change, and food-versus-biofuel related case studies and scenarios.

This study presents a new process-based sugarcane model, intended for applications from site to global scale. It is included as a module in the LSM Agro-IBIS (KUCHARIK; BRYE, 2003) which allows coupling of the LSM to atmospheric models, thereby permitting the simulation of bi-directional interactions between atmosphere and the sugarcane cropping system.

2. METHODOLOGY

2.1. Model description

2.1.1. Biogeophysical processes represented in Agro-IBIS

All crops represented in Agro-IBIS share the same physical and biophysical equations to simulate energy and mass balance within the natural ecosystem. Here we provide a concise summary of these processes, the complete equations used by the land surface models IBIS (Integrated Biosphere Simulator) and Agro-IBIS are fully documented in Foley et al. (1996) and Kucharik and Brye (2003). Agro-IBIS solves a set of equations to simulate energy, water, carbon, and momentum exchange between soil, vegetation (canopy and root system) and atmosphere. The physical equations operate over a one-hour time step. Other processes such as carbon allocation and phenology operate on scales from daily to yearly. Solar radiative balance in the surface is resolved using the two-stream approximation for each plant functional type (PFT), individually considering the direct and diffuse radiation in two wavebands (visible and near-infrared) - additional details are discussed in Section 3.1.

Agro-IBIS considers two canopy layers for natural vegetation types: an upper layer for trees and a lower one for grasses and shrubs. Only one layer (the lower) is considered when a crop is assigned. Turbulent flux and wind through the canopy are simulated using a simple logarithmic profile. An empirical linear function of wind speed is used to estimate turbulent flux between the soil (or snow) and the lower vegetation canopy. With the inclusion of the sugarcane module Agro-IBIS has 16 PFTs in total: 12 natural and four crops (soybean, maize, wheat, and sugarcane).

Hydrological processes simulated within the model include precipitation interception and retention by canopy, surface puddle formation, infiltration, water flux between the soil layers, deep percolation, evaporation from soil surface and from intercepted water by canopy, and canopy transpiration. In the current simulation, eight soil layers (from the top 12 m) were used to resolve hourly heat and water flux into soil. The soil module integrates the Richard’s equation to calculate the change of the liquid soil moisture, while the vertical flux of water is modeled according to Darcy’s Law. Soil texture and organic matter content in each layer, and differences between layers, influence one-dimensional water flow. Canopy transpiration is coupled to the photosynthesis through stomatal opening. Nitrogen cycle considers N fertilization, deposition, fixation, mineralization, plant uptake, and leaching. The current model version accounts for leaf nitrogen effects on photosynthesis.

The carbon cycle depends on atmosphere, canopy and soil conditions. Agro-IBIS simulates ecosystem carbon cycle through net primary production (NPP), heterotrophic respiration, and organic matter decomposition. Canopy physiology is characterized within the model in the following way: photosynthesis and stomatal conductance are calculated using the Farquhar-Ball-Collatz equations (BALL et al., 1987; COLLATZ et al., 1992; FARQUHAR et al., 1980). Gross photosynthesis rate (Ag) is a function of absorbed photosynthetic active radiation (APAR), intrinsic quantum efficiency, intercellular CO_2 concentration (which depends on atmospheric CO_2 concentration, stomatal regulation, and leaf boundary layer conductance), maximum capacity of Rubisco enzyme (V_{max}), and leaf temperature. The Ag relation with these quantities varies according to vegetation type (e.g., trees, shrubs, C3 and C4 grasses and crops). Two stress functions (water and nitrogen) also affect Ag. The water stress function is based on soil water content in the root zone - the contribution of each layer to the overall plant water stress being weighted by the soil layer root fraction. The Nitrogen stress function is dependent on the amount of available inorganic nitrogen in soil and on water availability for transpiration. This function accounts for the reduction of nitrogen transport from soil to leaves as soil water potential drops. Leaf maintenance respiration depends on V_{max} and leaf temperature, and root and stem maintenance respiration are functions of the total live carbon in the organs and their respective temperatures. Finally, NPP for each PFT is given by Ag less the respiration of the three organ systems (root, leaf and stem), and is further reduced by a coefficient to account for the fraction of carbon lost due to growth respiration (KUCHARIK et al., 2000). Weather (climatic) conditions affect photosynthesis through clouds (surface incident radiation), temperature (e.g., Rubisco Carboxilization), water vapor pressure (e.g., stomatal conductance), wind speed (turbulent CO_2, heat, and water fluxes) and precipitation (soil moisture conditions).

Agro-IBIS explicitly includes carbon flow between vegetation, detritus, and soil organic matter pools (KUCHARIK et al., 2000). Following the framework of Verberne et al. (1990), the model simulates microbial growth as a function of available litterfall biomass, root turnover, soil organic matter, and soil texture. Microbial activity dependents on an Arrhenius function of hourly temperature (LLOYD; TAYLOR, 1994) and water-filled pore space (LINN; DORA, 1984) – representing modifications of the original CENTURY model equations (PARTON et al., 1987). Root profiling functions designate where fine root and soil carbon are most likely to reside in the soil profile. These profiles allow soil moisture and temperature values to be weighted by depth according to carbon and microbial biomass. Leaves, wood and fine root biomass detritus are divided separately between three litter pool compartments (decomposable, structural, and lignified) according to theirs C:N ratios.

Agro-IBIS assumes that annual biomass and fine root turnover of the previous year are divided into equal daily increments in the current simulation year, that all living root biomass die during harvest, and that all root biomass enter into soil carbon pools immediately after harvesting. However, during sugarcane harvest most of non-millable cane (immature top portions of stalk) and leaves may be either burned (as occurs for most of harvested sugarcane in Brazil) or left over soil (usually when the sugarcane is mechanically harvested). Another notable difference from other crops is that the sugarcane root system dies partially immediately after harvest, and the remaining root biomass is completely or partially replaced in the subsequent months after ratooning (SMITH et al., 2005). To account for these specific physiological and management characteristics of the sugarcane cropping system some modifications to the model were therefore necessary: First, daily root biomass decayed along the crop cycle was added to soil in the same day. Second, it was assumed that 17% of root biomass dies immediately after harvest, and the remaining biomass is assumed to decay in the subsequent 60 days (figures based on the review of SMITH et al., 2005). Additionally, the impact pre-harvest fire on carbon balance was considered, as discussed in the next section.

2.1.2. Crop management

The original Agro-IBIS model included only annual crops (maize, soybean, and wheat), while sugarcane is a perennial crop. Moreover, the sugarcane growth period (between planting and harvest) is quite variable, depending on climate and plant cultivars. Usually, sugarcane is harvested between 12 and 24 months after planted (namely planted crop), and in the following years (usually from two to six years) it re-grows from the stubble (known as the ratoon crop) and is harvested every year. In the continental United States (mainly in Florida and Louisiana), planted sugarcane grows for 12 to 18 months before harvest, and two ratoon crops are typically grown (GREENLAND, 2005). In Hawaii, planted crop may grow continuously for 2 or 3 years before harvest. In Brazil two different groups of hybrids are planted: one that matures 12 months after planting and one that maturates after 15 to 18 months. The harvest season goes from May to November in Southeast Brazil and from September to February in Northeast Brazil.

In a typical 18 month cycle in southern Brazil (illustrated in Figure 2), the sugarcane is planted in the first months of the year, between January and May and is harvested from May to November of the following year. Four to five ratoon crops are grown in consecutive years with an associated drop in productivity in the ratoon cycles. After the last ratoon cycle the land is either left fallow for some months or a summer crop is cultivated, after which the soil is managed for the next crop cycle.

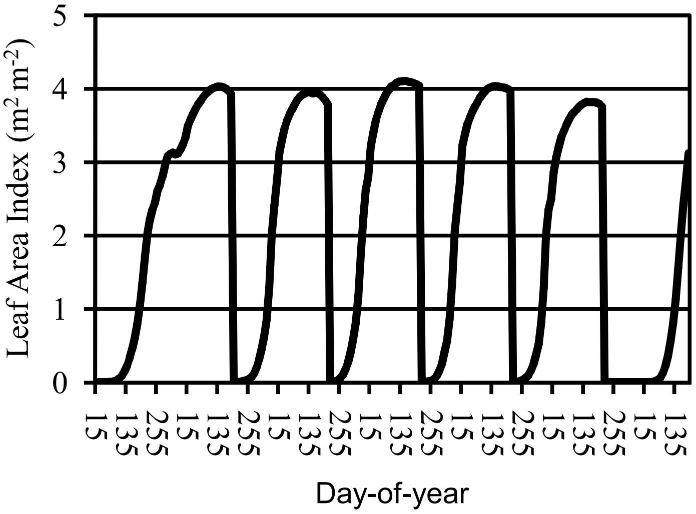

The bracket in the horizontal axis represents the harvest window, and the middle of the bracket represents expected harvest date.

Figure 2 – Example of Leaf Area Index (LAI) development (simulated) for a typical sugarcane crop cycle (one plant cycle and four ratoon cycles) in southeast Brazil.

For all crops, planting date may be either prescribed or determined by the model. The model's decision to plant a crop is based on three conditions: The 10-day running averages of both daily mean air temperature and minimum temperature must be higher than specified thresholds. Furthermore, planting cannot take place before a specific date based on the typical growing season across the region in question. All three conditions must be met for planting to take place.

For annual crops, harvest takes place when both GDD (Growing Degree Days, thermal time in units of °C per day accumulated since planting) is equal or higher than GDD_m (GDD to achieve physiological maturity) and the day during the integration is higher than the specified day-of-year set as the earliest harvest day. For sugarcane, the harvest takes place in a specified harvest window between a minimum and maximum day-of-year (represented in Figure 2 by a bracket). Then, as in the other crops, sugarcane is harvested (in the harvest window) when GDD reaches GDD_m. In the literature, a base temperature between 8°C and 15°C is used to compute the GDD for sugarcane (KEATING et al., 1999) and Agro-IBIS uses a base temperature of 12°C. Since the model is designed to run from site to global scale, the thermal time to reach physiological maturity is not a pre-specified crop GDD_m but is calculated interactively during integration based on the normal planted crop growth period, days between planting, and expected harvest date (date centered between maximum and minimum harvest days). A first approximation for GDD_m is calculated based on annual climatology, for a given grid point, and then for every crop cycle this value is interactively updated based on temperature during integration. A maximum defined hybrid GDD_m can also be specified. After the sugarcane is harvested the consecutive ratoons are grown until the same harvest window.

In addition to the plant and harvest controls, the crop management module also considers nitrogen fertilization and irrigation. Fertilization is applied every planting date, and the amount of N per hectare applied is pre-specified, either fixed for each crop type or varied according to an input file. However, due to the lack of information on level of fertilization, soil nitrogen content, impact of pre-harvest fire on nitrogen emission/deposition in the present simulations, the nitrogen impact on photosynthesis was not considered and nitrogen stress functions was considered as non-limiting. Irrigation, if applied, can be either specified or calculated during the integration based on average daily water content in the soil (the amount of water applied to a managed ecosystem was computed on a daily basis).

Another important difference between the sugarcane agro-ecosystem and the other crop systems is the employment of fire by the time of harvest. Cane harvest is achieved in two main ways. The cane can be manually cut, which is normally associated with pre-harvest fire. Alternatively, it can be mechanically harvested with or without pre-harvest burning. In both cases, fire may be use before harvesting to increase efficiency (RIPOLI et al., 2000) and after harvest to clean the ground. The model considers the possible use of fire through the incorporation of one parameter that determines the use of fire during the harvest process. It is quite difficult to predict the litter during any crop cycle (INMAN-BAMBER et al., 2002), and to estimate the biomass left after harvest with pre-harvest fire may be even more difficult and variable (in time and space). In the present simulation, we considered the simple hypotheses that in case of fire only 25% of straw (total dead leaf and meristem) is incorporated into litter (based on SOUZA et al., 2005), and the remaining is assumed to be burnt.

2.1.3. Phenology and carbon allocation

Agro-IBIS has different methodologies to account for the phenology and carbon (C) allocation of crop and natural ecosystems. For annual crops, Agro-IBIS considers three key growth stages controlled by GDD: (i) from planting to leaf emergence; (ii) from leaf emergence to end of silking; (iii) from grain fill to physiological maturity. Each phenological stage is characterized by different C allocation fractions to the four specific C pools (i.e., leaf, stem, root, and grain) based on CERES-Maize and EPIC models (KUCHARIK; BRYE, 2003). Leaf emergence occurs when the GDD is higher than a specific percentage of the GDD_m. The second phase goes from leaf emergence to end of silking, at which time most of NPP goes to leaves and roots. The third phase, grain fill to senescence, is characterized by grain formation.

For the sugarcane crop, a new carbon allocation scheme was implemented. Based on an analysis of the two main international sugarcane crop models, APSIM-Sugarcane (KEATING et al., 1999) and CANEGRO (SINGELS; BEZUIDENHOUT, 2002; SINGELS et al., 2005) we developed a new Agro-IBIS carbon allocation scheme, drawing heavily on the CANEGRO model equations. Our first modification in the original CANEGRO C allocation set of equations was to consider the allocations as a function of GDD, instead of accumulated biomass (since it is not possible to know the typical crop biomass for all grid points). As mentioned above, in grain crops such as soybean and maize, daily NPP is allocated to the four carbon pools: leaves, roots, grains and stem. Analogously, in the sugarcane module daily NPP is allocated to four carbon pools: leaves (A_l), roots (A_r), stem sucrose (A_{suc}), and structural stem (A_{stc} - stem fibre plus non-sucrose material). First, daily NPP is divided between aerial (A_a - all above ground biomass), roots (A_r), and stem (A_{stm}) C pools, where A_{stm} includes A_{suc} plus A_{stc}:

$$A_a = (1 - A_{rm}) \times min\left[1, 1 - \mathrm{e}^{-(\mathrm{Rd} \times \mathrm{RM})}\right] \tag{1}$$

$$A_{stm} = min\ [(1 - A_{lm} - A_{rm}), A_a \times max\ (0,\ F_1,\ F_2)\ ] \tag{2}$$

$$F_1 = (RM \times C_{lstem}) - (I_{lstem} \times C_{lstem}) \tag{3}$$

$$F_2 = 1 - \mathrm{e}^{[(\mathrm{RM} \times C_{estem}) - (I_{estem} \times C_{estem})]} \tag{4}$$

$$RM = 100 \times \left(\frac{GDD}{GDD_m}\right) \tag{5}$$

Where *RM* is the crop relative maturity, R_d is the root decline coefficient, and A_{rm} and A_{lm} are the minimum fraction of carbon allocation to roots and leaves, respectively. *RM* expresses the evolution in GDD along the crop cycle in a scale that ranges from 0 to 100. It normalizes the spatial variability of GDD and is computed for each grid point interactively. F_1 and F_2 are the linear and exponential functions that describe stem allocation; the maximum value of these two functions composes the allocations to stems (A_{stm}) (Figure 3). These functions are based on the principle that carbon allocation to stems is nearly linear in the beginning of sugarcane growth and then follows a logarithmic profile for the rest of crop cycle (see KEATING et al., 1999 for some observational evidence).

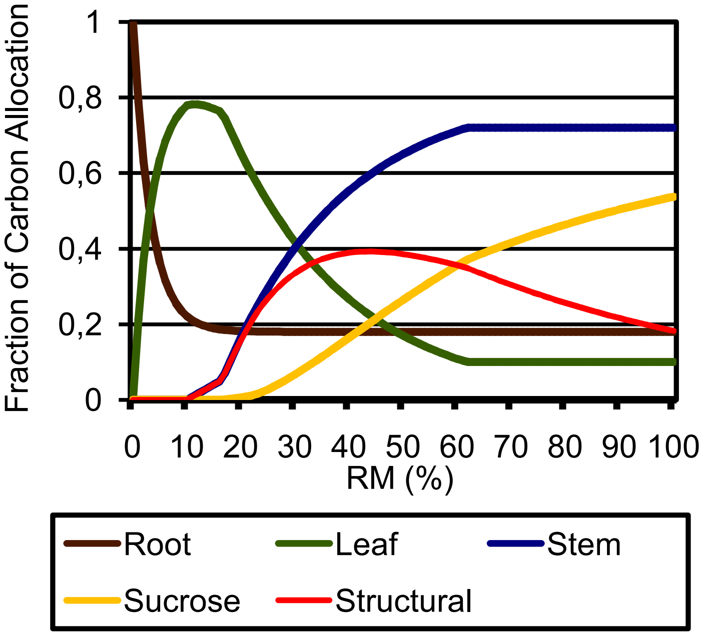

Figure 3 – Fractional carbon allocation to the different carbon compartments in sugarcane along crop cycle: root (brown line), leaves (green line), stalk (cane - blue line), structural (red line), and sucrose (yellow line).

F_1 (Eq. 3) is a linear function of RM (Eq. 5), C_{lstem} is the angular coefficient of F_1 and the product between C_{lstem} times I_{lstem} determines the GDD for which F_1 is greater than 0.0. Therefore, C_{lstem} and I_{lstem} define when carbon starts to be allocated to structural stem (when F_1 and F_2 are lower than 0.0 they are not accounted for A_{stm} – there is no negative allocation). For example, a I_{lstem} (linear intercept point) of 10 (Figure 3) signifies that the linear allocation to A_{stm} starts when RM is equal to 10 (or GDD is equal to 10% of $\mathrm{GDD_m}$).

F_2 (Eq. 4) is an exponential function of RM (Eq. 5). The coefficient C_{estem} determines the exponential function F_2 and the product between C_{estem} and I_{estem} establish the GDD for which F_2 is greater than 0.0; therefore, C_{estem} times I_{estem} defines when the exponential function F_2 can potentially (i.e., F_2 greater than F_1 and zero) direct carbon allocation to the structural stem. For example, I_{lstem} (exponential intercept point – RM for which F_2 is equal to zero) is equal to 15 in Fig. 3, meaning that F_2 is greater than zero from RM higher than 15 (or GDD higher than 15% of $\mathrm{GDD_m}$).

In addition, root allocation (A_r) is the complement of A_a to the unit, and leaves allocation (A_l) is given by (A_a - A_{stm}). Following the same form of functions, carbon allocated to stem (Eq. 2) is then partitioned between stem sucrose (A_{suc}), and structural stem (A_{stc}) following the set of equations:

$$A_{suc} = A_{stem} \times max(0,\ F_3,\ F_4) \qquad (6)$$

$$F_3 = (RM \times C_{lsuc}) - (I_{lsuc} \times C_{lsuc}) \qquad (7)$$

$$F_4 = 1 - \mathrm{e}^{[(\mathrm{RM} \times C_{esuc}) - (I_{esuc} \times C_{esuc})]} \qquad (8)$$

Additionally, temperature is known to alter carbon allocation in sugarcane. For example, under cold or mild dry conditions carbon is allocated preferentially in the sucrose form (SINGELS; BEZUIDENHOUT, 2002). However, in this initial version of model we focus on simulating total stem (cane) production. Currently, temperature influences sugarcane physiology (e.g., influencing photosynthetic efficiency, stomatal opening) and, if daily temperature drops below 0^{o}C, leaf area index (LAI) is linearly reduced until -5.6^{o}C, at which point the crop dies (GREENLAND, 2005; KEATING et al., 1999).

Finally, the carbon content of each organ is updated on a daily basis by accumulating the daily NPP allocated to each organ fraction and subtracting the organ turnover (considered to occur only for leaves and roots). Although leaf turnover in sugarcane depends on temperature, leaf age, light competition, and water stress (e.g., KEATING et al., 1999; SMITH; SINGELS, 2006), leaf and root turnover are simulated as the product between the carbon content in each pool and a constant turnover rate. Additionally, leaves are considered to decay if temperature drops below water freezing point. The physical proprieties of the canopy (e.g., reflectance, transmittance, canopy water storage and heat capacity) are modeled as a function of the carbon accumulated to leaves and stem, and LAI is given by the product of carbon in the leaf pool and a constant specific leaf area (SLA - $m^2.kg^{-1}$).

2.2. Validations and input data sets

Four different datasets of increasing spatial scale were used to validate the yield simulated by the sugarcane module: (i) micro-meteorological and biomass observations, obtained for one crop cycle (391 days) in northern São Paulo state (Brazil), (ii) yield from two consecutive ratoons grown with three different irrigation regimes at an experimental site at Kalamia estate, Australia; (iii) sixteen years of yield data for the four largest sugarcane producing meso-regions in the Brazilian state of São Paulo; (iv) annual average yield over 31 years for the U.S. state of Louisiana.

2.2.1. São Paulo state experimental site

First we validate the model against micro-meteorological measurements made over a sugarcane plantation (*Saccharum* spp., cultivar SP83-2847) during one ratoon cycle (second ratoon) cultivated in a commercial area of 351 ha. This area belongs to the Santa Rita Mill in the Sao Jose do Pulador farm (Farm n.^{o} 27), near the city of Luiz Antonio, Sao Paulo state, Brazil (21^{o}38'S, 47^{o}47'W, elevation 552 m). The ratoon cycle goes from 14 April 2005 to 10 May 2006 (second and third harvest, respectively). The crop was planted with an inter-row spacing of 1.5 m and attained a height of 3m at harvest. As there were no observations for the preceding cycle, the days between 38 and 104 of 2005 are only shown as reference points for the analyzed crop cycle and were not considered in the analyses.

The granulometric analysis showed a mean (first 2 m) soil composition of 22% of clay, 3% of silt and 74% of sand. The regional climate is typically warm and wet in the summer, and mild and dry in the winter (see TATSCH et al., 2009). Both temperature and precipitation show a marked annual cycle. The mean monthly temperature varies between 19^{o}C in June and 24^{o}C in February, with a mean annual temperature of 22^{o}C. The mean monthly rainfall is about 50 mm in the dry season and reaches more than 200 mm during wet season.

The model was forced with meteorological data from an automatic weather station. The data were sampled every 10s and registered as 10 min averages in a datalogger (CR10X, Campbell Systems). Hourly average means of air temperatures, global solar radiation, relative humidity, surface pressure, wind speed, and daily precipitation were used as input for the simulation. Tatsch et al. (2009) provide a detailed description of the experimental site, meteorological and biomass datasets. Micro-meteorological measurements made over sugarcane at the São Paulo state are also described in Cabral et al. (2003) and Rocha et al. (2000). Validations include sensible heat flux (H), latent heat flux (λE) and carbon dioxide flux (which is compared against modeled net ecosystem exchange NEE) derived from the eddy covariance technique. In all simulations, model was integrated considering 11 soil layers, with a total soil depth of 2.5 m.

2.2.2. Kalamia estate experimental site

The site level data at Kalamia estate (19.6^{o}S, 147.4^{o}E), northeast Australia, is used to evaluate model biomass and evapotranspiration (ET) for two consecutive ratoon crops grown with three different irrigation regimes. Sugarcane was planted on 27 September 1999 and harvested on 25 September 2000. The first ratoon covers the period from 25 September 2000 to 18 July 2001, and second ratoon from 18 July 2001 to 16 August 2002. This field experiment used three irrigation schedules once the crop was fully established: two treatments were irrigated 1-3 times a week to replace water used at an estimated rate of $1.00xET_0$ ($1.00ET_0$) and $1.25xET_0$ ($1.25ET_0$), where ET_0 is the reference evapotranspiration (ALLEN et al., 1998). The third treatment was conventional furrow irrigated (FRW), providing at least 70 mm of water when a soil available water deficit of about 70 mm had developed. This deficit was calculated using the estimated evapotranspiration rate of $1.25xET_0$.

The experimental site was divided into 12 plots, 4 replications for each treatment. Each plot consisted of nine rows 1.52 m apart and 39 m long. All plant and soil measurements were taken from the four inner irrigated rows (net plot). Complete information about the field experiment is given by Inman-Bamber and Attard (2008). Simulations were forced with daily meteorological observations made at the site, and daily irrigation (see Figure 4, gray columns) follows the daily field observations for each treatment.

2.2.3. São Paulo mesoregions

A second set of simulations were compared with sixteen years (1990-2005) of modeled and observed sugarcane yield for the four mesoregions (= a cluster of municipalities used for statistical purposes) (Figure 4) in São Paulo state (Brazil). São Paulo is the largest sugarcane producer in Brazil, producing around 60% of total Brazil production (http://www.conab.gov.br/conabweb/). Data were collected by the governmental institution IBGE (Brazilian Institute of Geography and Statistics – http://www.sidra.ibge.gov.br). The IBGE mesoregions and the four largest mesoregions sugarcane producers are (1) Ribeirão Preto, (2) São José do Rio Preto, (3) Bauru, and (4) Araçatuba. The combined output of these four mesoregions represents ~40% of total Brazil production. The Agro-IBIS terrestrial grid (0.5^o) points considered in the simulations are based on the 1995 gridded sugarcane fractional cover (Figure 4). Simulations were forced by the Climate Research Unit (CRU) version 3.0 climate data set (http://badc.nerc.ac.uk) monthly maximum and minimum air temperature, precipitation, vapor pressure, and cloud cover (from 1982 to 2005), and the period between 1990 and 2005 was used to compare simulations against IBGE's yield estimation. Growing season was considered as one year starting/ending in August (for the São Paulo state). Climatic means and anomalies also consider one year average, from August to August; anomalies were derived from the 1990-2005 mean.

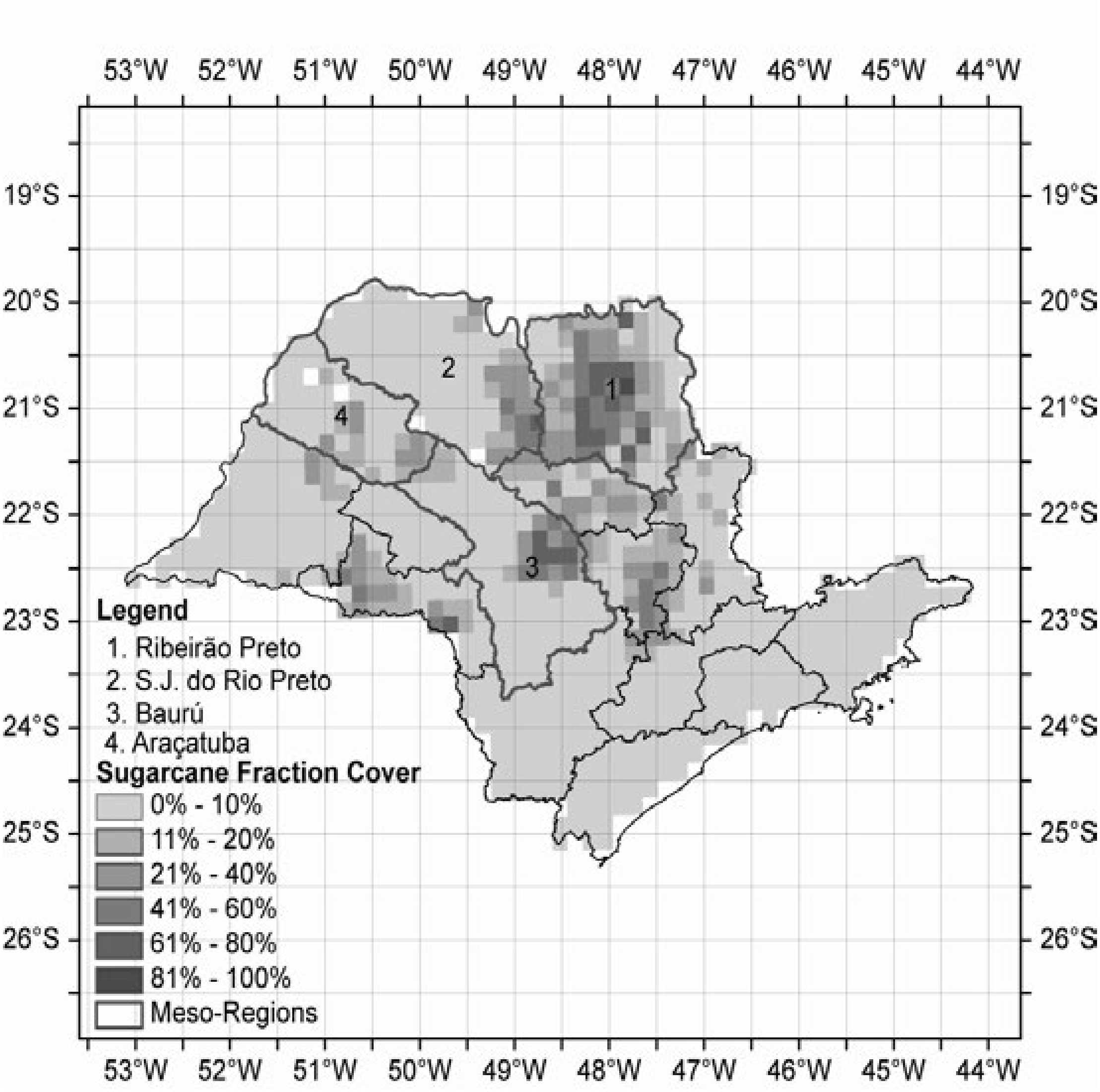

The four mesoregions considered in the simulations are indicated by the numbers: (1) Ribeirão Preto; (2) São José do Rio Preto; (3) Bauru; (4) Araçatuba. Grid corresponds to the terrestrial grid used by Agro-IBIS (0.5o), which is the same as the CRU monthly climate dataset. Percentage under sugarcane cultivation (fractional cover) for each pixel (~0.16o) is plotted over the map (shaded field), based on the IBGE's 1995 census.

Figure 4 – São Paulo state map (Brazil) showing the mesoregions (municipalities cluster) according to IBGE's (see text) municipal aggregation.

2.2.4. Louisiana state

The third validation compares simulated results over a 0.5º x 0.5º grid against statewide yield for the U.S. state of Louisiana. Estimated yields were taken from Greenland et al. (2005). The dataset was produced by the American Sugarcane League and the period used for validation goes from 1963 to 1993. The model was integrated from 1958 to 1993 for all Louisiana State grid points and state yield average considers the grid points following the main sugarcane cultivated area presented by Greenland et al. (2005).

The simulation used version 2.1 of the CRU data set (Mitchell and Jones, 2005) and the National Centers for Environmental Prediction National Center for Atmospheric Research (NCEP-NCAR) reanalysis (KANAMITSU et al., 2002) in conjunction with a weather generator to produce hourly data. Daily variability for each meteorological variable were derived from the NCEP climate reanalysis considering the monthly values from the CRU data set for the period from 1963 to 1993. This improve the representation of daily weather events, which impacts the crop growth, while preserving the monthly variables values from the CRU data set. Finally, hourly average values of air temperature, precipitation, relative humidity, solar radiation, and wind speed were derived using the WGEN (RICHARDSON; WRIGHT, 1984) weather generator. Kucharik (2003) provides the full details of this methodology to obtain sub-daily meteorological variables to force Agro-IBIS.

3. RESULTS AND DISCUSSION

3.1. São Paulo state experimental site

3.1.1. Leaves biomass and radiation fluxes

Hourly radiation intercepted by canopy is given by the nature of incident radiation (direct or diffuse), incidence angle, leaves and stem area index, radiation extinction coefficient, and leaves and stem reflectances at each waveband. The process adopted to adjust reflectances followed three interactive steps: (i) adjustment of carbon allocation to leaves pool (i.e., LAI); (ii) adjustment of radiation extinction coefficient, and; (iii) adjustment of green and brown (dead) leaves reflectances.

The simulation underestimated green leaves dry matter in the first and later stages of crop cycle, while dry matter in the more photosynthetic active phase was in close concordance with the observed data (Figure 5). LAI field observations were not as frequent as dry matter ones and LAI was therefore indirectly estimated by the product of green leaves dry matter and the specific leaf area (SLA) measurement (5.7 $m^2 \cdot kg^{-1}$) on a dry matter base or approximately 13.5 m^2 per kg of carbon (TATSCH et al., 2009). However, this estimation introduces a degree of uncertainty in the LAI validation because SLA is usually variable in time, whereas the calculation was based on a single measurement of SLA during the period of the investigation. SLA is also quite dependent on cultivar and environmental conditions, and the 5.7 $m^2 \cdot kg^{-1}$ observed is relatively low compared with typical range of published values (e.g., PELLEGRINO, 2001; PINTO et al., 2006). Assuming the observed total green leaves maximum (average) of 5.5 $t \cdot ha^{-1}$ (Figure 5 – dry matter) results in an observed maximum LAI of around 3.1 $m^2 \cdot m^{-2}$ (0.55 $kg \cdot m^{-2}$ times 5.7 $m^2 \cdot kg^{-1}$), while the maximum simulated green LAI was 2.7 $m^2 \cdot m^{-2}$ (Figure 5).

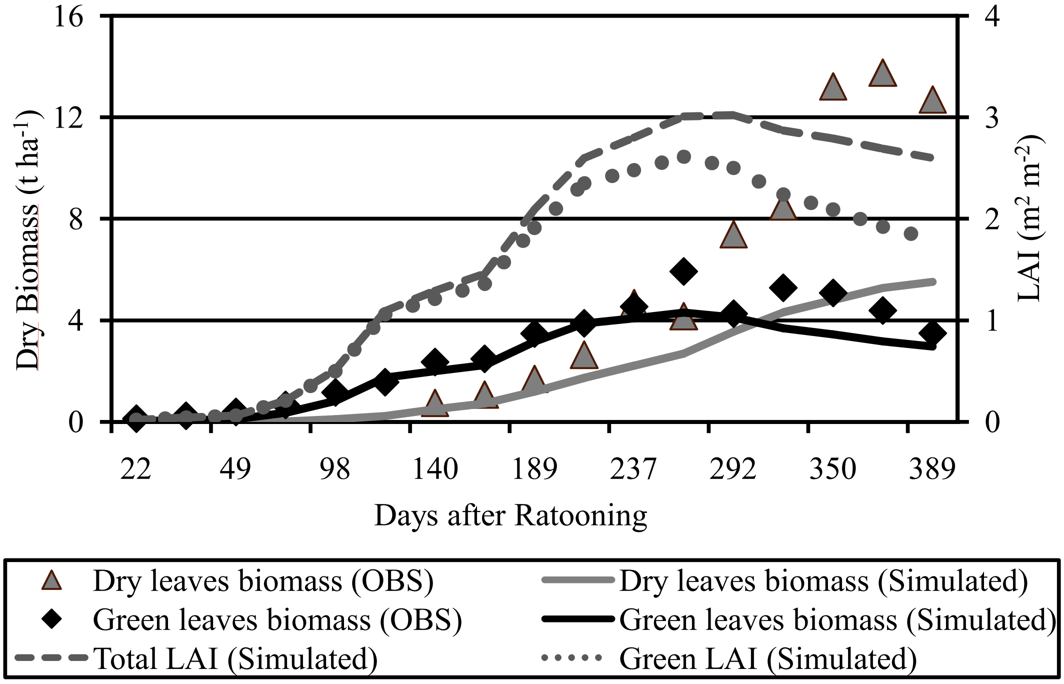

Figure 5 – Observed (symbols) and simulated (lines) dry matter accumulation in green (black) and dead (dark gray) leaves during the ratoon cycle. Simulated total (green plus attached dead, dark gray dashed line) and green (light gray dotted line) LAI are displayed in the right axis.

Agro-IBIS simulates leaf decay as the product between foliage biomass and a constant turnover time. Even using a relative low (related to the others cultures) value for average leaf resident time (175 days) simulated dead leaves dry biomass is underestimated. Although the simulated value is much lower than observed, the observed and simulated dead leaves values are in the range of values reported in literature (e.g., THOMPSON, 1978; ROBETENSON et al., 1996; INMAN-BAMBER et al., 2002).

Two different procedures were adopted to calibrate the radiation extinction coefficient, both based on the assumption that LAI and SAI (stem area index) had been accurately simulated. Radiation extinction coefficient (K_e) in IBIS depends on three parameters (leaf orientation, transmittance and reflectance) and two diagnostic variables (LAI and SAI). Leaf orientation along with LAI determines the leaf projected area in the beam direction. Typically, leaf angle departure (χ_L) is assumed to be -0.5 for C4 species (χ_L ranges from -1 for vertical leaves, 0 for randomly oriented, 1 for horizontal leaves).

The sensitivity of the simulated reflectance was assessed for phase 2 and phase 3 using two different values for χ_L (-0.5 and -0.2) (Figure 6). Phase 2 is the full canopy phase (from day 270 of 2005 to 48 of 2006) and is characterized by low albedos. Phase 3 is the senescence period (from day 68 to 130 of 2006) during which green/brown LAI gradually reduces/increases, and albedos increase. The best fit to the observed values was achieved when χ_L was set at -0.2.

Simulated total solar radiation flux (R_s) attenuation by canopy resulted in an estimated K_e (radiation extinction coefficient) of 0.55 (Figure 7a). Although 0.55 is relative high in the range of sugarcane observations (0.37-0.53) reported by Park et al. (2005), it is consistent with their observation that tropical locations are characterized by high K_e. It is also important to note that K_e differs between crop classes, cultivars, and soil and climatic conditions (ROBERTSON et al., 1996; PARK et al., 2005). The relationship between intercepted R_s and LAI (Figure 7b) is also consistent with other reported values (e.g., MUCHOW et al., 1999; PARK et al., 2005).

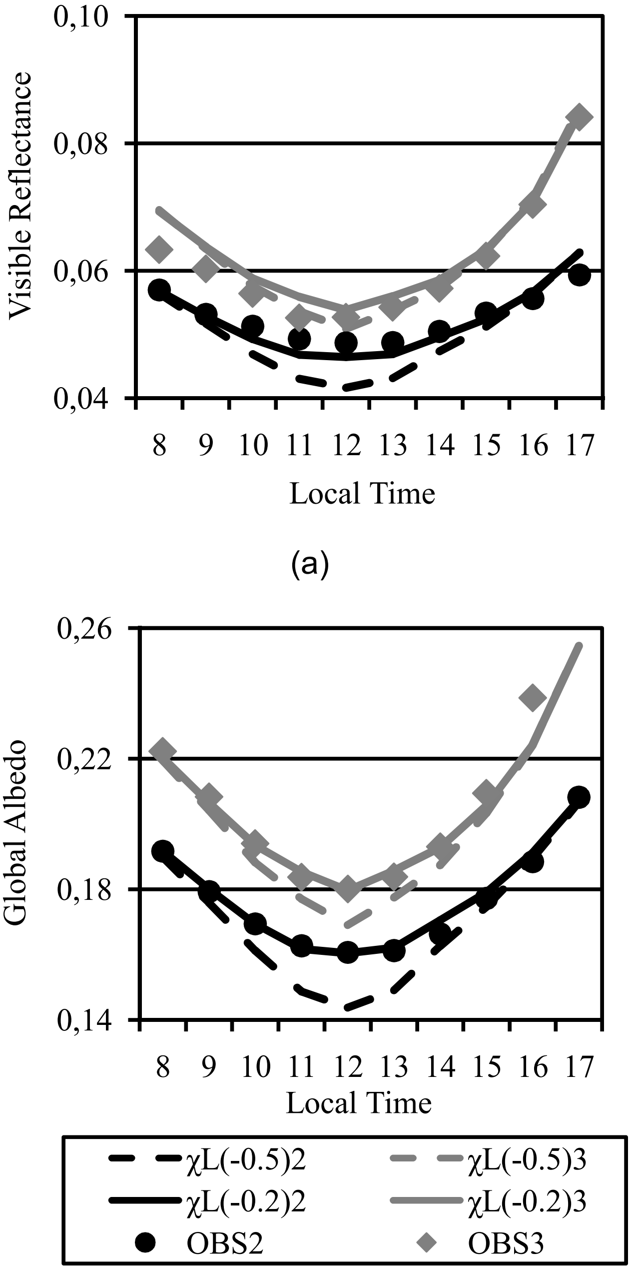

(a)

(b)

Figure 6 – Observed (symbols) and simulated (solid and dashed lines): (a) visible reflectance and (b) global solar albedo diurnal cycle averaged for two periods, full canopy (black) and senescence (gray) period. Simulations differ in the leaf angle departure (χ_L); see text for details.

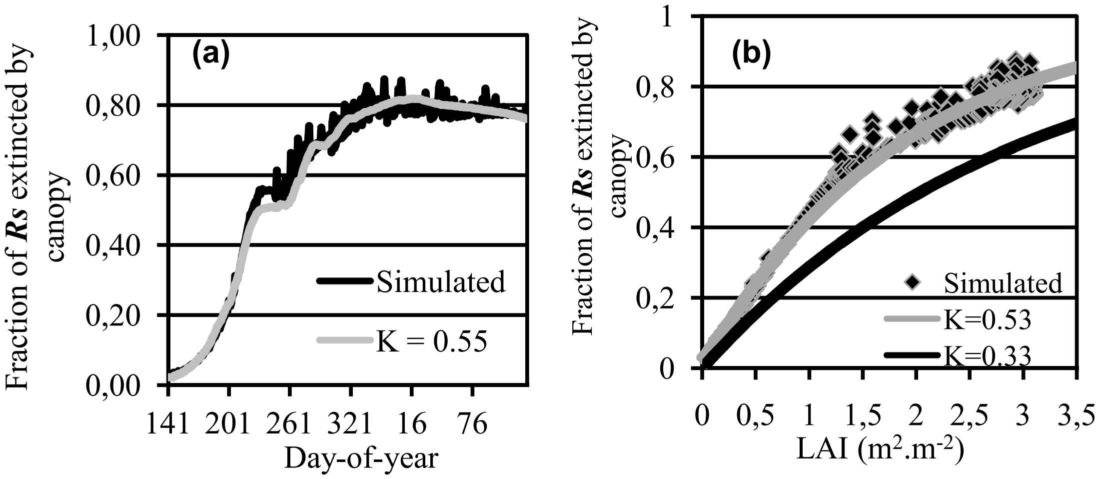

Figure 7 – Fraction of total solar radiation flux (R_s) extincted by canopy integrated by model (black line) along the crop cycle and analytical solution of analogous Beer-Lambert law (gray line) with extinction coefficient (K_e) of 0.55 (best fit to the simulated R_s extinction) (a); R_s extincted by canopy as function of LAI integrated by model (black symbol) and according to Beer-Lambert law using $K_e = 0.33$ (black line) and 0.53 (gray line); values of K_e reported by Park et al. (2005) (b).

The model produced a very close concordance between daily simulated and observed surface R_s and photosynthetic active radiation flux (R_p) reflectances (Figure 8) – solar radiation is separated in two wavelength bands (visible from 0.4 to 0.7 µm and near-infrared from 0.7 to 4.0 µm). In the day after harvest (day 108 of 2005) R_p reflectance leaps from 0.05 to 0.1 in both observation and simulation. Aerial biomass not harvested (top and leaves) was left over ground and burned around day 140, as seen by the drop in observed albedo (R_s reflectance). Although the model successfully simulates the increase in albedo after harvest, in the days between harvest and biomass burn the simulation somewhat deviates from observations (R_p reflectance). This is attributable to the fact that Agro-IBIS does not have a module to account explicitly the management of aerial biomass not harvested – leaves were considered to be burnt on the harvest day and any remaining meristem was incorporated into the litter pool. Field observations indicate that both reflectances remain high until the day the fields are burnt, probably because of straw left over ground, in contrast to simulated albedo that was derived from bare soil. After this initial stage, the simulation and observations show a similar pattern, indicating that R_s/R_p reflectances gradually increase/decrease as LAI develops. As LAI grows, simulated R_p reflectance increasingly approaches observations until it stabilizes at 0.05, when simulated LAI is around 2.0.

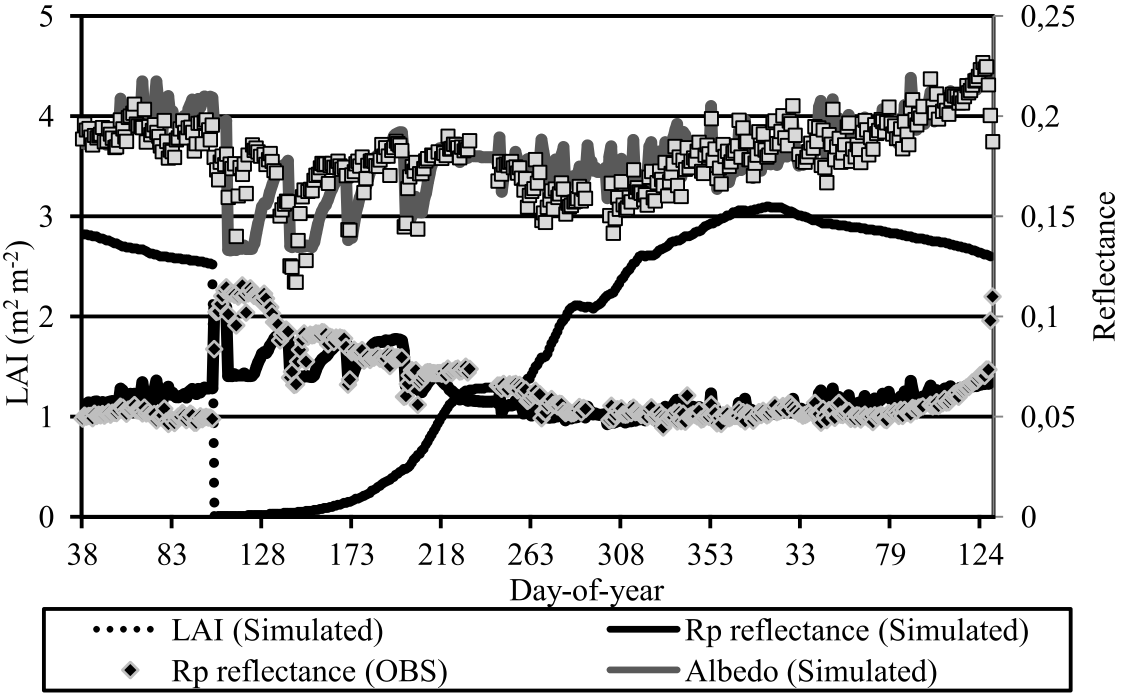

Figure 8 – Daily surface total solar radiation flux (R_s - dark gray) and photosynthetically active radiation flux (R_p - black) reflectances, observed (symbols) and simulated (solid lines) – right vertical axis scale. Total, green plus attached dead leaves, LAI (m^2 m^{-2} – black dotted line) simulated is plotted in the left axis scale. Period goes from day 38 of 2005 to 129 of 2006.

3.1.2. Carbon balance and evapotranspiration

The seasonal photosynthetic cycle is robustly simulated by the model, although daily variability is best simulated for the period of maximum assimilation (Figure 9). Another clearly observable pattern is that simulated NEE drops sooner and to a greater degree than observed values during periods with low precipitation (e.g. between days 10 and 40 of 2006). The underestimation in this period is the major contributor to the final diurnal average NEE bias (-6.44%, as inferred from the deviations of the cumulative curves – Figure 9).

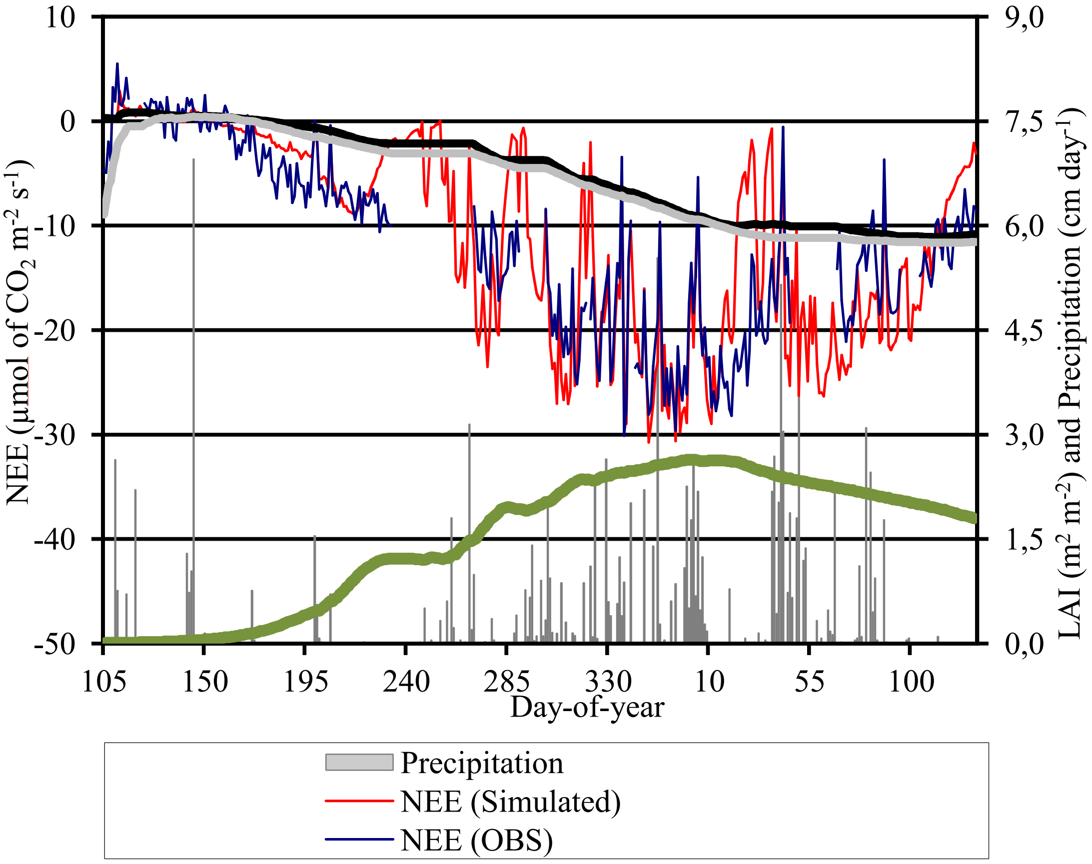

Figure 9 – Average diurnal (from 8 am to 18 pm, local time) CO_2 net ecosystem exchange (NEE - µmol of CO_2 m^{-2} s^{-1}) observed (blue line) and simulated (red line). Cumulative NEE observed (gray line) and simulated (black line) are also plotted in the left axis. Green LAI (m^2 m^{-2} – green dotted line) and observed precipitation (cm day^{-1} - background gray column) are plotted in the right axis scale. Period goes from day 105 (ratooning) of 2005 to 129 of 2006 (harvest).

Diurnal cycles of NEE (Figure 10) were divided in three periods: (1) initial growth (from day 124 to 233 of 2005); (2) crop growth maximum (from day 270 of 2005 to 48 of 2006), and; (3) crop growth decline (from day 68 to 130 of 2006). The gaps between periods being caused by a lack observations during these times (illustrated in Figure 9). In the initial period Agro-IBIS underestimated NEE (Figure 10), this being most apparent after midday. In the second period of the cycle, assimilation increases with R_p flux until 11.00 am and then gradually decreases after that (Figure 10). Although simulated and observed NEE show a high degree of concordance, modeled NEE tends to decreases relative to the observed data from 11.00 am to 4.00 pm. During the latter period the modeled results follow the observations closely throughout the entire diurnal cycle.

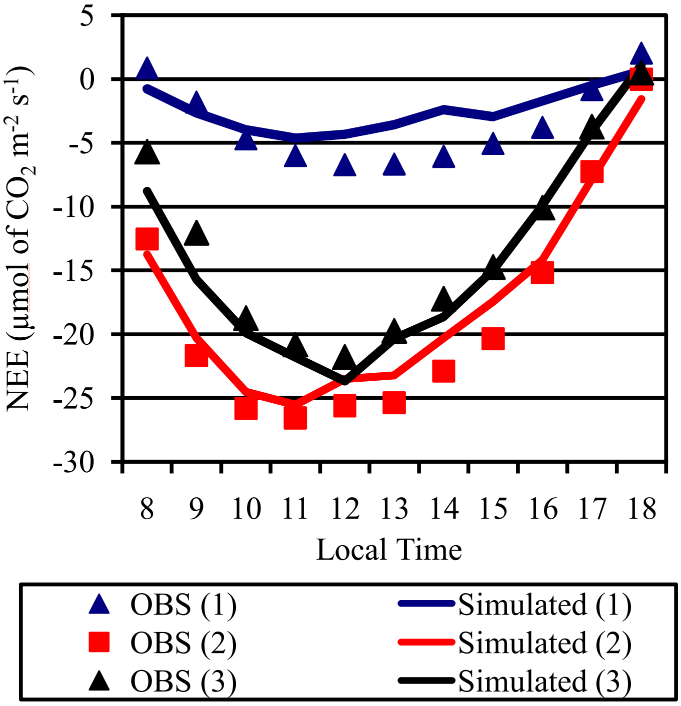

Figure 10 – Observed (symbols) and simulated (lines) average CO_2 net ecosystem exchange (NEE - µmol of CO_2 m^{-2} s^{-1}) diurnal cycle for three periods: (1) initial growth (blue line and symbol); (2) maximum crop growth rate (red line and symbol); and (3) decline crop growth rate (black line and symbol).

Simulated hourly NEE shows a similar relationship with air temperature to observed NEE (Figure 11a). NEE grows exponentially with temperature until a maximum assimilation around 27°C, and then drops shutting down for temperatures higher than 35°C. It is important to note that other factors also affect this relationship. For example, relative humidity (*h*) also has a strong influence over NEE, and *h* tended to vary from 20% to 40% for temperatures of about 35°C. The model also accurately simulates the relationship between photosynthesis and *h* (Figure 11b). When simulated NEE is plotted against observed NEE (Figure 11c), the general fit of the model is good (R^2 = 0.69, relative bias -6.6%).

The model gives a generally robust simulation of ET (Figures 12a and 12b) as demonstrated by a strong correlation with observed values (R^2 = 0.87), although there is a tendency of overestimation (0.32 mm day^{-1} on average) – with the exception of periods of soil exposure when LAI is below 1.0 m^2 m^{-2}. ET bias tends to be especially high in days following precipitation events, and tends to drop during dry periods. This pattern is driven by the soil water stress function, which tends to reduce photosynthesis and ET as soil dries.

The model tends to overestimate ET when temperatures are higher than 25°C (Figure 13a). Despite this bias, the simulated relationship is once again generally concordant with observed values. Both simulation and observation are characterized by a maximum ET at approximately 30°C, while maximum NEE occurs at about 27°C, reflecting a decrease in the water use efficiency above this value. The relationship between ET and *h* is also well captured by the simulation (Figure 13b). Maximum ET tends to increase when *h* ranges from 20% to 50% and decrease linearly when *h* varies from 50% to 100%. Dispersion between observed and simulated ET (Figure 13c) presents low dispersion (R^2 = 0.79) and systematic deviation for observed ET > 0.3 mm hr^{-1}; linear regression has a slope coefficient of 1.13.

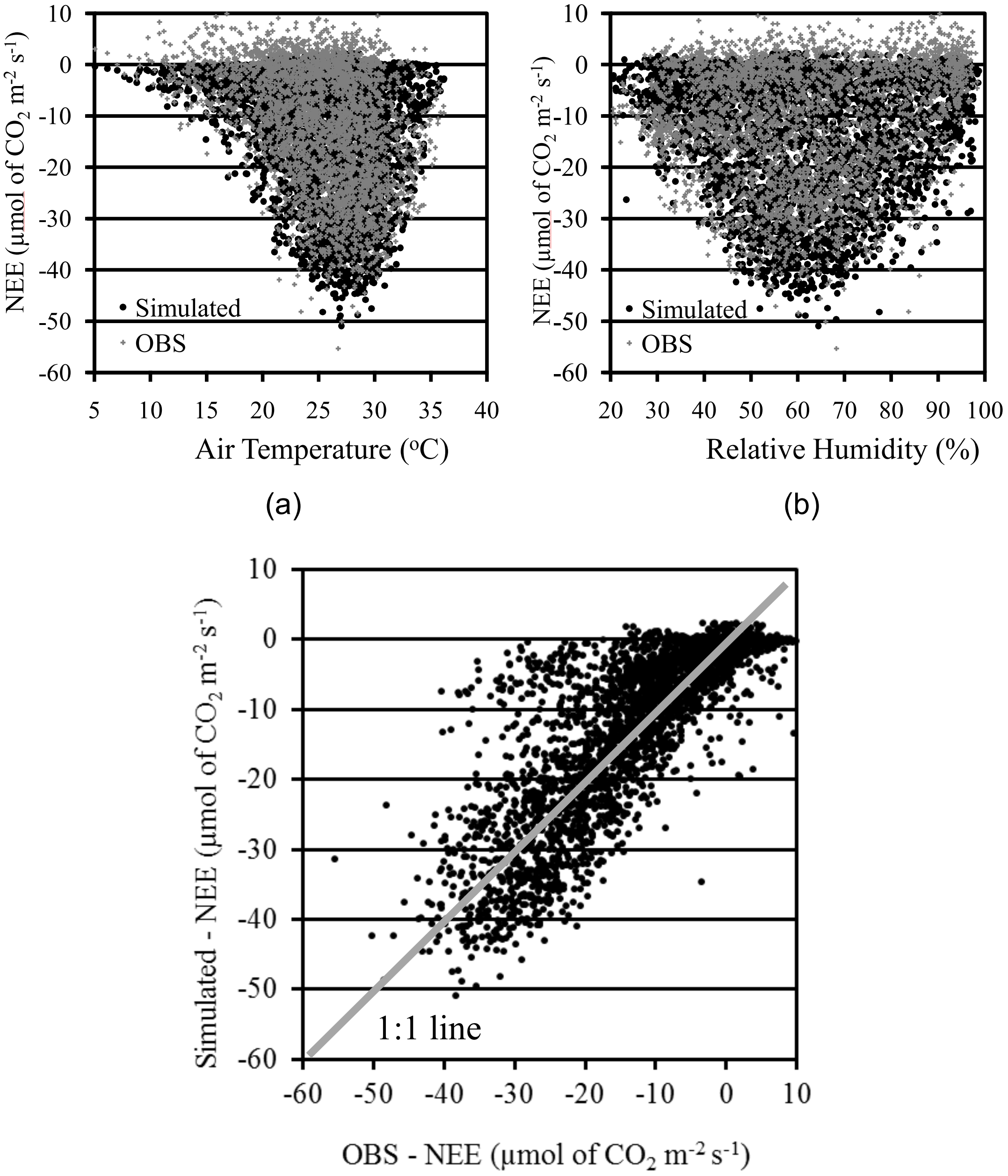

(a)

(b)

(c)

Figure 11 – Dispersion diagram between hourly net CO_2 ecosystem exchange (NEE - µmol of CO_2 m^{-2} s^{-1}) and air temperature (above canopy – reference level), observed (gray symbol) and simulated (black symbol) (a); same as (a) for NEE and relative humidity (%) (b); dispersion diagram between hourly observed and simulated NEE (c).

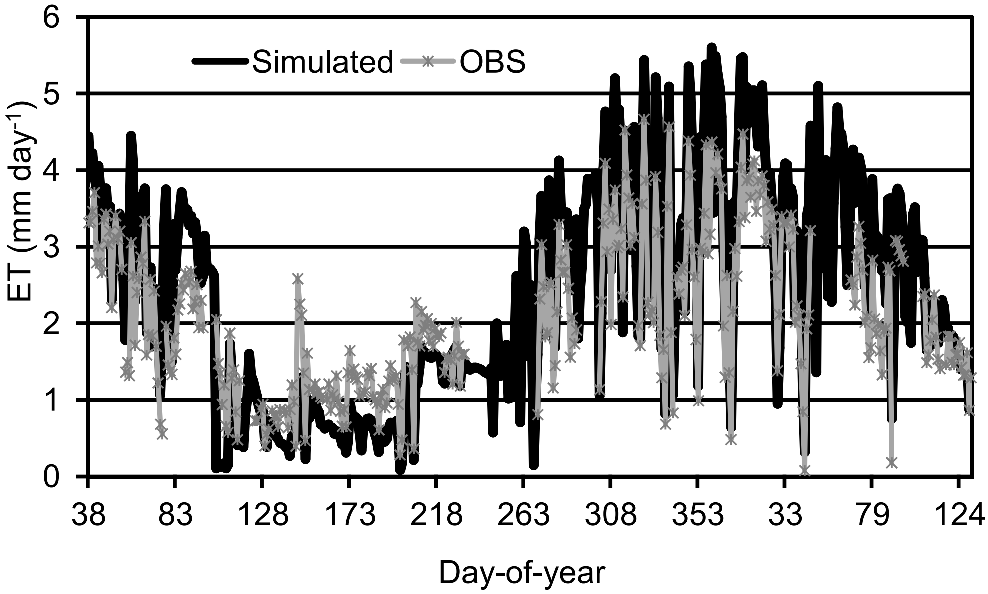

(a)

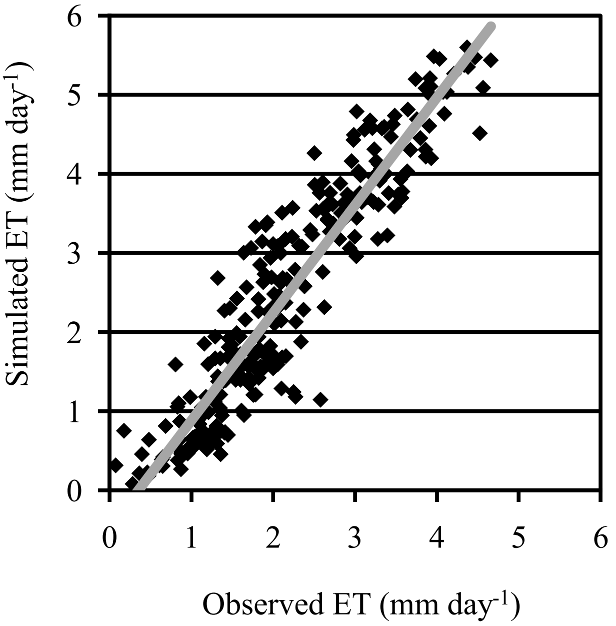

(b)

Figure 12 – Daily ET (evapotranspiration – mm day^{-1}) observed (gray line) and simulated (black line) (a); dispersion diagram between observed and simulated daily ET (mm day^{-1}) (b).

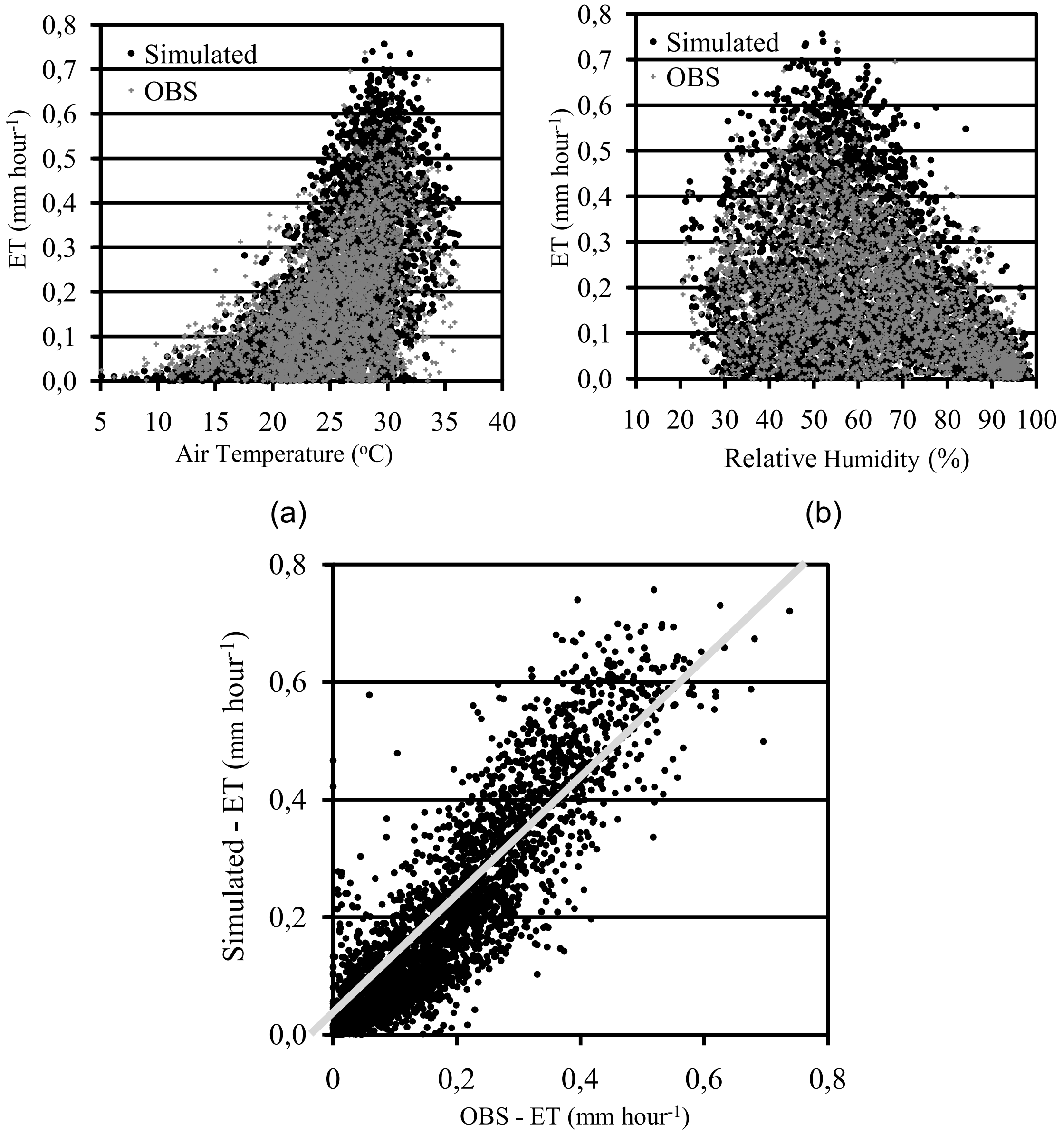

(a) (b)

(c)

Figure 13 – Dispersion diagram between hourly ET (evapotranspiration – mm hour^{-1}) and air temperature (above canopy – reference level), observed (gray symbol) and simulated (black symbol) (a); same as (a) for ET and relative humidity (%) (b); dispersion diagram between hourly observed and simulated ET (c).

ET underestimation resembles NEE and air temperature relationship (Figure 14a), suggesting that this relationship is (as expected) related with stomatal opening. Maximum ET bias occurs at temperatures around 30°C, indicating a concomitant effect of temperature via water vapor pressure deficit. However, there is no clear relationship between ET bias and *h* (R^2 = 0.003; Figure 14b), with the maximum observed bias for *h* between 40 and 70% (coincident with temperatures of around 30°C).

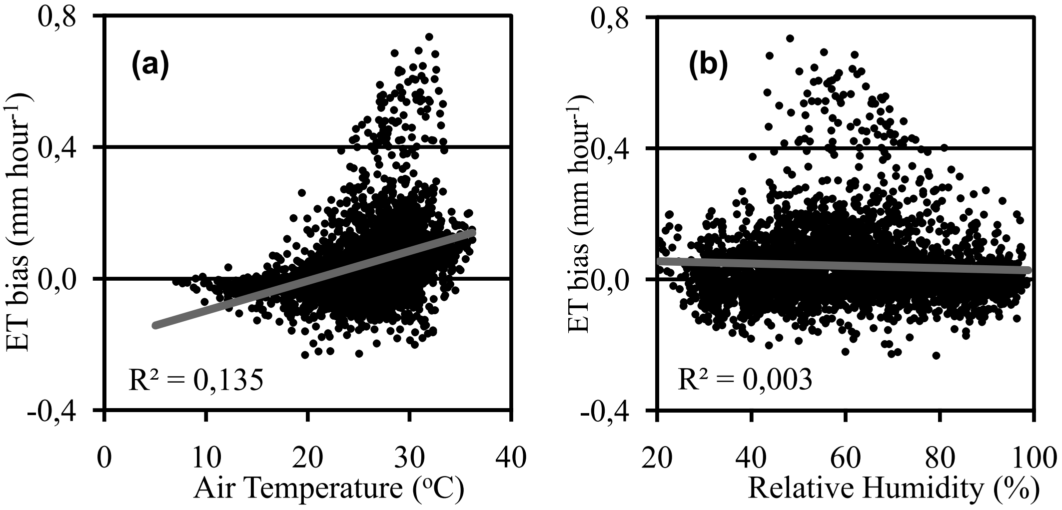

Figure 14 – Dispersion diagram between ET (evapotranspiration – mm hour^{-1}) bias against: (a) air temperature (°C) and (b) relative humidity (%).

The modeled relationship between NEE and absorbed solar radiation is generally similar to observations (Figure 15). NEE over absorbed solar radiation (AR_s) increases almost linearly until a maximum is reached around day 340 of 2005 (some days before green leaf biomass reaches its maximum – Figure 5, DAR 237), and model overestimates this increase after day 249. Although result is close to the observations during the maximum photosynthetic active period, the model tends to be over sensitive to dry events. During the final phase of crop cycle, the model tends to overestimate the rate of NEE/AR_s – with exception of final days of the cycle when the model responds more intensely to water shortage. Most of literature reports radiation use efficiency (RUE) as the rate of aerial dry biomass per MJ of solar radiation intercepted (e.g., 1.59 g MJ^{-1} for ratoon crop; ROBERTSON et al., 1996). This cannot be derived from observations in the current study as solar radiation just below green canopy was not measured. Modeled NPP over-absorbed solar radiation by total green leaves was 1.9 g MJ^{-1} during the full canopy period, which is consistent with potential (non stressed) 2.12 g MJ^{-1} value reported by Singels and Bezuidenhout (2002) and field values reported by Muchow et al. (1999).

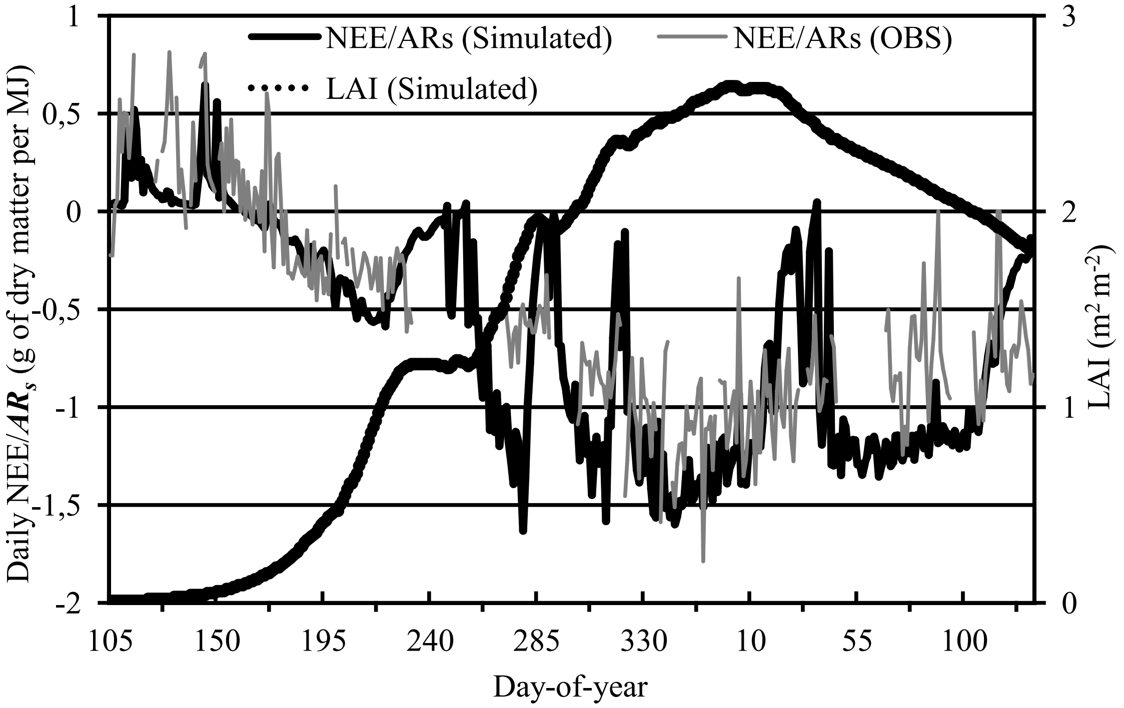

Figure 15 – Observed (gray line) and simulated (black line) daily rate between CO_2 net ecosystem exchange (NEE - in dry matter base) and surface absorbed solar radiation (AR_s – MJ m^{-2} day^{-1}). Simulated LAI (m^2 m^{-2} – black dotted line) is plotted in the right axis scale.

The ratio between simulated NEE and ET, a measure of water use efficiency, follows observations closely across the entire crop cycle (Figures 16a and 16b). NEE/ET starts to drop around day 147 then decreases faster until day-of-year 210. This decline continues until about day-of-year 336, which coincides with maximum green leaves biomass. Observed and simulated dispersion between NEE and ET present similar linear regressions (Figure 16b).

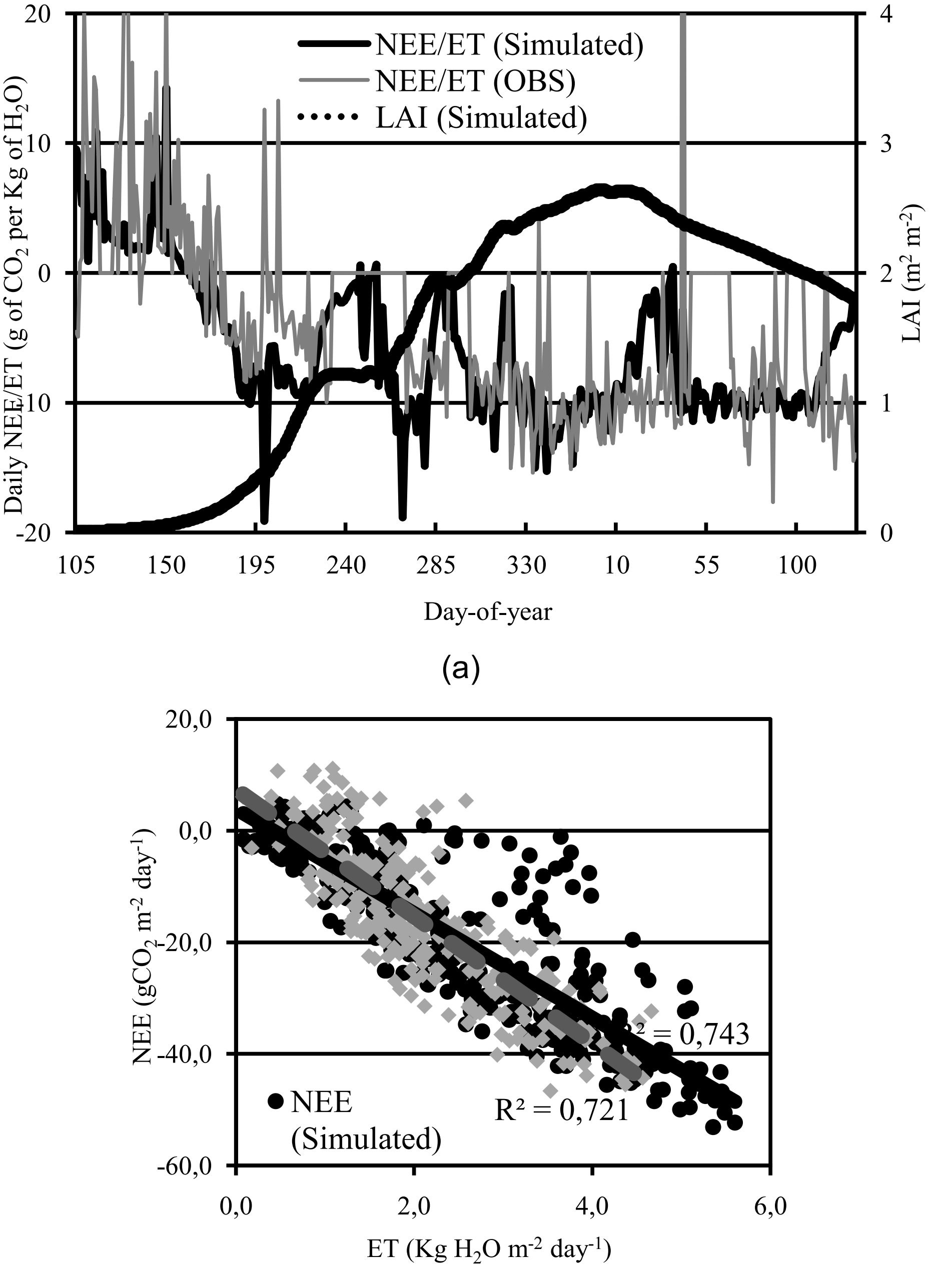

(a)

(b)

Figure 16 – Observed (gray line) and simulated (black line) daily CO_2 net ecosystem exchange (NEE - gCO_2 m^{-2} day^{-1}) over evapotranspiration (ET – kg m^{-2} day^{-1}). Simulated LAI (black dotted line - m^2 m^{-2}) is plotted on the right axis scale (a); dispersion diagram between daily NEE (gCO_2 m^{-2} day^{-1}) and ET (kg m^{-2} day^{-1}) (b).

Dry biomass observations made in the micro-meteorological experiment go from June 5th of 2005 (22 days after ratooning - DAR) to May 10th of 2006, two days before harvest (389 DAR). Total green leaves dry biomass is accurately simulated, with a slight underestimation from the middle until the end of cycle (Figure 17). Total dead leaves dry biomass is overestimated at the beginning of cycle and underestimated from 140 DAR onwards. Cane biomass is robustly simulated for most points along the crop cycle. The main deviations occurred from day 327 to 375, with final biomass converging again with observations (final relative bias equal to -6.23%). Total aerial biomass is underestimated from 140 DAR onwards. Most of the underestimation is related to total dead leaves biomass, which was relatively high compared to other published locations (e.g., ROBETENSON et al. 1996; INMAN-BAMBER et al., 2002).

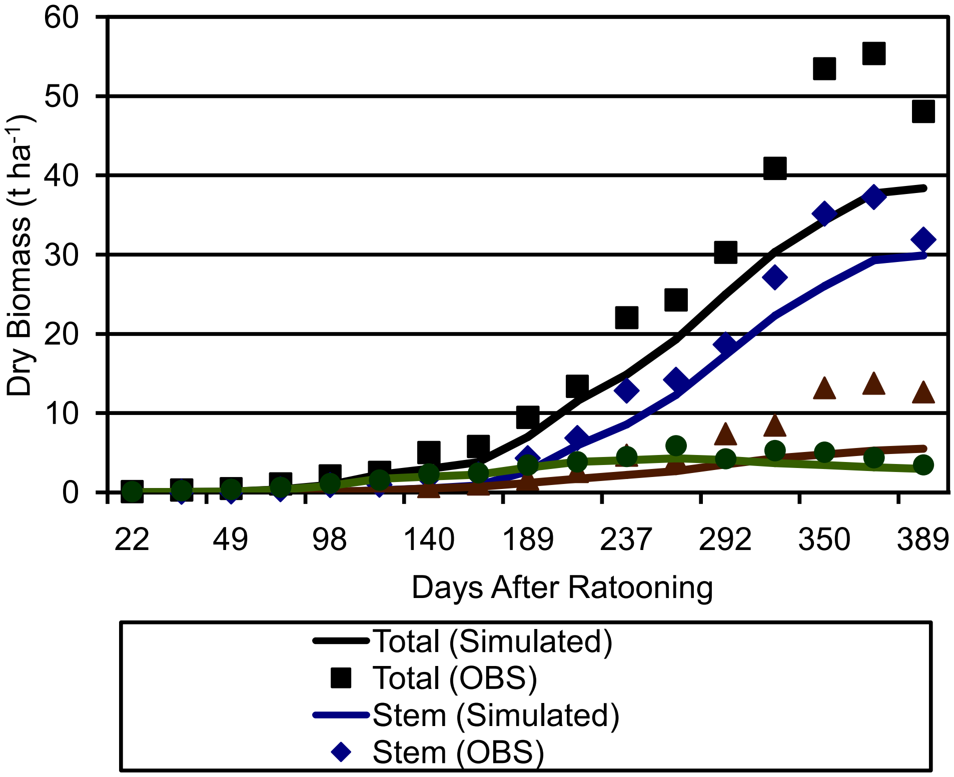

Figure 17 – Observed (symbols) and simulated (lines) dry biomass (t ha^{-1}) accumulated along the ratoon cycle: total aerial (black), cane (blue); dead (dry) leaves (brown), and green leaves (green).

3.1.3. Energy balance

Net radiation (R_n) is underestimated by the model when soil is exposed (Figure 18). As the canopy grows simulated R_n converges with observations, and bias tends to be less than 5.0%. Even though the simulation follows the observed decrease in the rate between R_n and AR_s when soil is more exposed (consistent with the high soil heat accumulation during the day and increase of thermal radiation lost during night, and less transpiration), Agro-IBIS overestimated the long wave radiation lost in the initial crop growth stage. Considering the entire cycle, the model shows a relative bias of -6.5% (R^2 = 0.97).

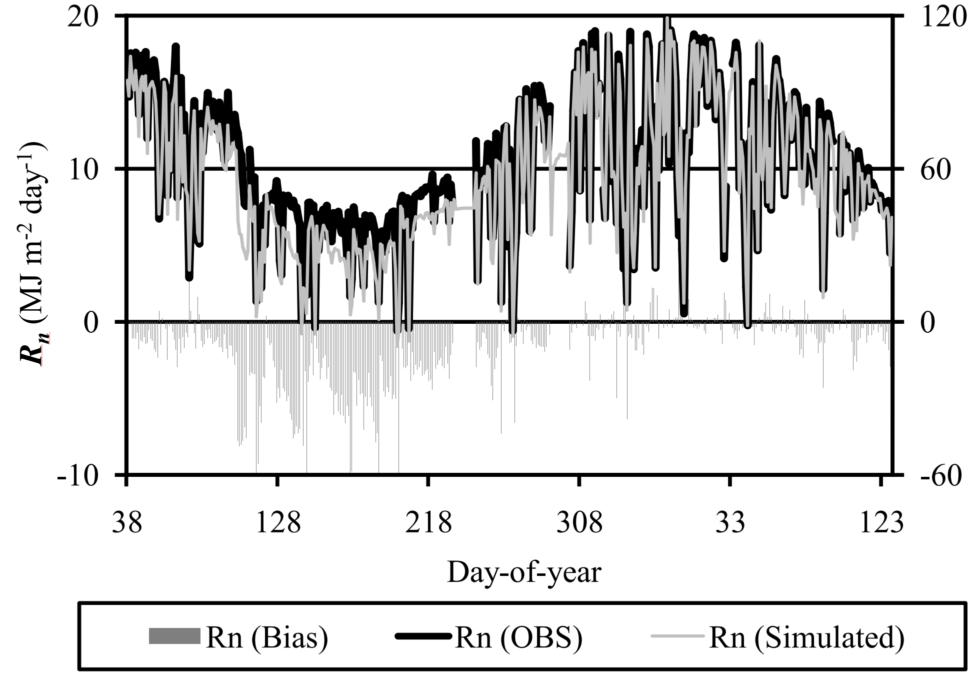

Figure 18 – Observed (black) and simulated (gray) daily net radiation (R_n). Light gray columns shows net radiation relative bias (%, scale in the right axis).

Daily soil temperature is accurately simulated by model (Figure 19). However simulated soil heat flux diurnal cycle shows a more pronounced amplitude (21d), highlighting the importance of considering a specific layer of dead biomass over the soil – thereby connecting the litter fall biomass with the energy and water balance. Despite a large amplitude in the diurnal cycle, the seasonal and diurnal variability of soil temperature is consistently simulated. The soil temperature overestimation during the period when vegetation cover is non-existent (Figure 19) was also reported by Kucharik and Twine (2007).

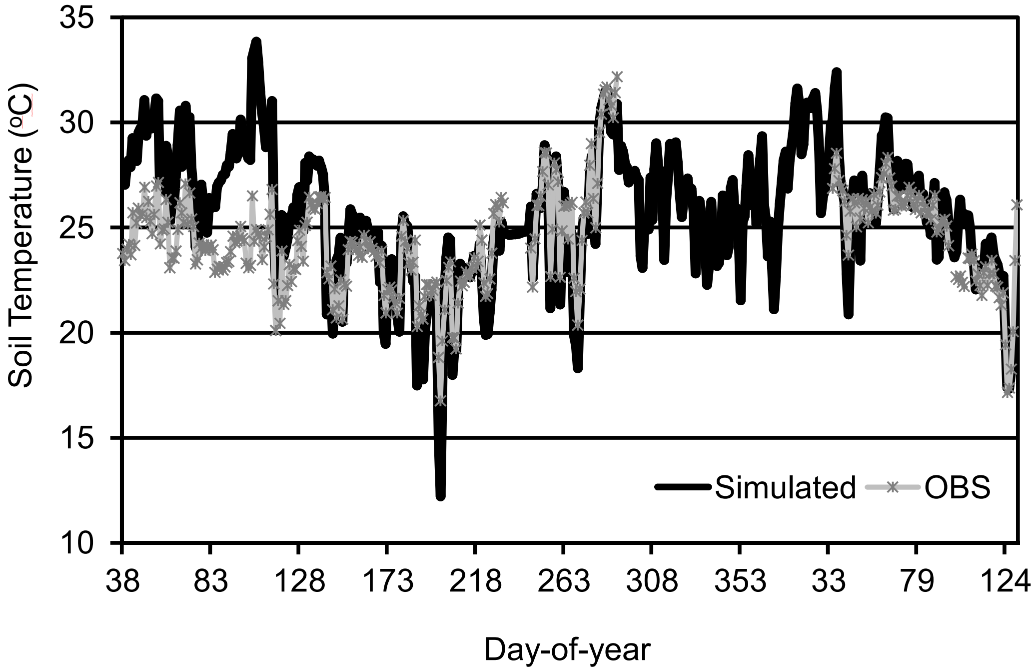

Figure 19 – Observed (at 2 cm, gray line) and simulated (first soil layer – 2.5 cm, black line) soil surface temperature (^oC).

After harvest, the Bowen ratio (β) rises rapidly from around 0.5 to 2.0 (Figure 20). During this period β is strongly coupled to precipitation and is observed to drop after rain events and to increase as soil dries. As the canopy develops, β tends to decrease linearly until it reaches an average minimum of about 0.5 (observed) and 0.35 (simulated). Although the simulated energy partition seasonal cycle is consistently simulated, β is overestimated for low LAI and underestimated for high LAI. The dispersion diagram of observed and simulated *H* and *λE* (Fig. 20b) shows that the model systematically under/overestimates *H/λE* with a relative bias of -10.5% (*H*) and 14.8% (*λE*) and an R^2 equal to 0.68 (*H*) and 0.87 (*λE*).

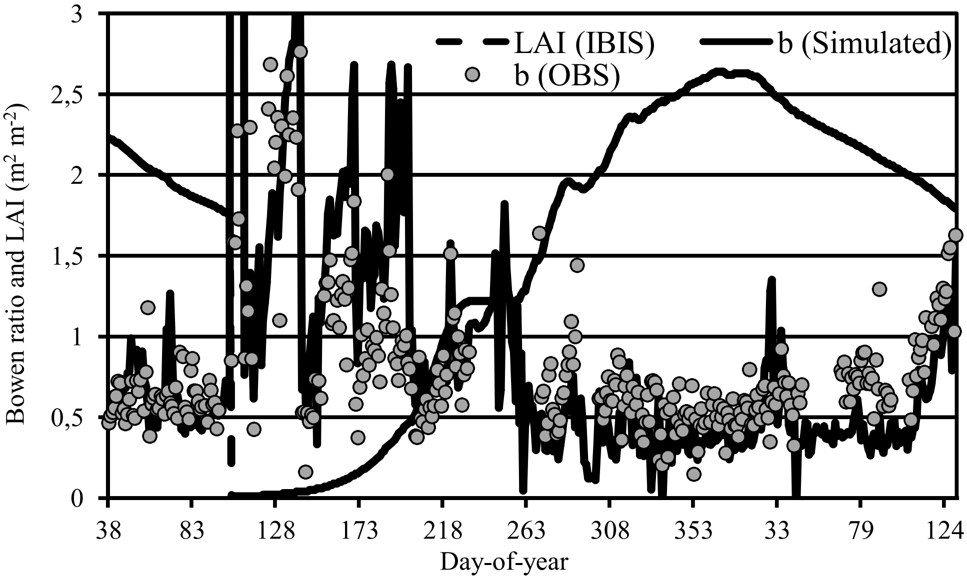

(a)

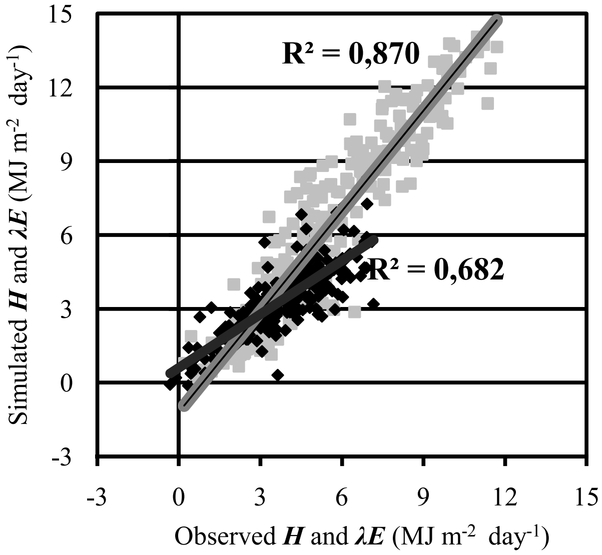

(b)

Figure 20 – Observed (black line) and simulated (gray line) daily Bowen ratio (*β* - Sensible over Latent heat fluxes). Simulated LAI (m^2 m^{-2}, dotted black line) is shown as references (a); dispersion diagram between daily observed and simulated Sensible (*H* - black symbol) and Latent (*λE* - gray symbol) heat fluxes (MJ m^{-2} day^{-1}) – linear regressions and R^2 are shown for each dispersions (b).

The diurnal cycle of energy balance components (Figure 21) was separated in two periods: (i) canopy development (from day 124 to 233 of 2005), (ii) full canopy cover (from day 270 of 2005 to the end of crop cycle). Average R_n is accurately simulated in both periods, showing only small deviations in the first phase when the soil is exposed.

In the first crop period, the model simulates too much heat being conducted into the soil during the morning and, consequently, soil heat flux (G) is overestimated (Figure 21d) and H (Figure 21c) is underestimated. Only after 12.00am do G and H converge with observations. Excess heat accumulated in the soil is conducted back to the surface around sunset, and most of it is lost as long wave radiation after sunset (Figure 21a). λE is underestimated during the entire diurnal period (Figure 21c).

During the second crop phase when the canopy is fully developed, λE is overestimated after 09.00am, with a maximum bias at 01.00am – interestingly, the same period when NEE is underestimated. G is also overestimated, although to a lesser extent, from sunrise until 12.00am (into soil), and after 03.00pm (out of soil). H is underestimated from 08.00am to 01.00pm, but is accurately simulated for the remaining period. However, the correct simulation of H after 01.00pm is probably a reflection of the overestimation of soil temperature (due to the morning soil heat flux overestimation), and not from correct energy partitioning.

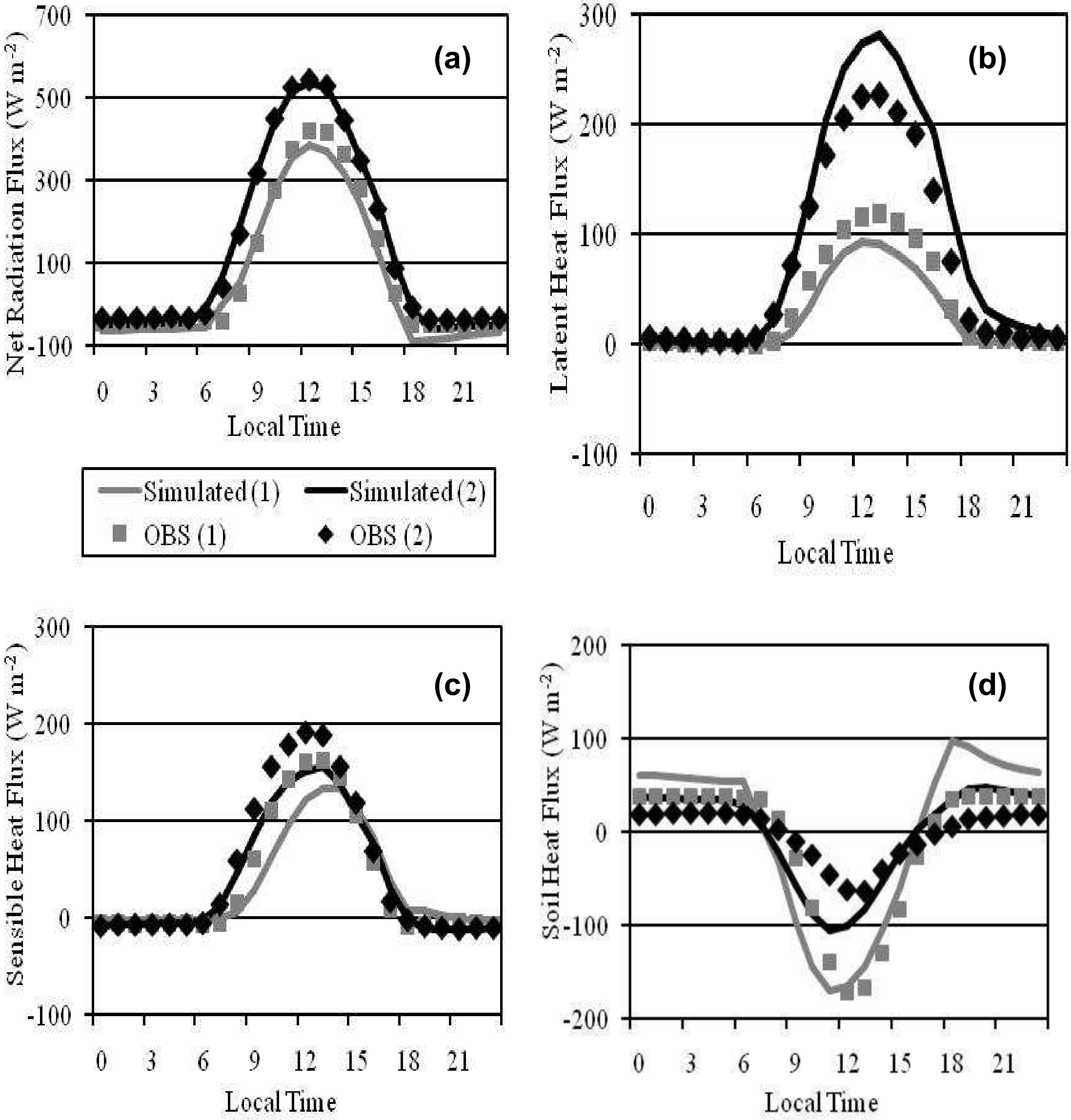

Figure 21 – Observed (symbols) and simulated (lines) diurnal cycle energy balance components averaged for two periods: (1 – gray) during canopy development; (2 - black) for full canopy cover. (a) Net radiation (R_n – W m^{-2}), (b) Latent heat flux (λE – W m^{-2}), (c) Sensible heat flux (H – W m^{-2}), and (d) Soil heat Flux (G – W m^{-2}).

3.2. Kalamia estate experimental site

The final simulated LAI was very similar to observed for the three experiments (Figure 22), although simulated LAI deviated from the observed value at 199 DAR (days after ratooning) for the 1.00ET$_0$ and FRW treatments. In the second ratoon cycle there were no LAI observations. Here, the LAI simulations showed a greater difference between 1.25ET$_0$ and FRW than in the first cycle, in part because initial LAI development occurred in a relative drier period in the second ratoon (see black bars in Figure 23a-c).

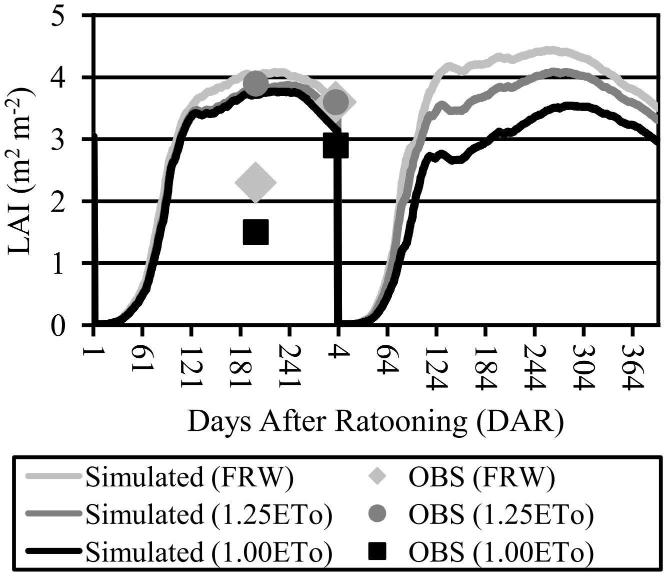

Figure 22 – Observed (symbols) and simulated (lines) LAI (m^2 m^{-2}) over two consecutive ratoon cycles for the three irrigation treatments: 1.00 x ET0 (black), 1.25 x ET0 (dark gray), and furrow irrigation (light gray).

The model slightly underestimated ET at the beginning of ratoon cycles, but closely followed estimated values (gray symbols) in the middle of the cycle (Figure 23a-c). In the first ratoon cycle, ET increased quickly during the first months due to high solar radiation flux and rapid LAI development (The first ratoon starts in September and the second one in July). At the end of the first cycle the different irrigation regimes resulted in significant ET differences. The last irrigation application in the $1.00ET_0$, $1.25ET_0$, and FRW treatments were 33.9 mm (236 DAR), 43.8 mm (236 DAR), and 112.6 mm (241 DAR), respectively. In the days following these last irrigations, ET decreased exponentially in both $1.00ET_0$ and $1.25ET_0$, while ET decreased linearly in FRW (mainly following a reduction in radiation rather than soil moisture). Although the model slightly overestimated ET at the end of first ratoon cycle in $1.00ET_0$ and $1.25ET_0$, responses of ET to different irrigation regimes were robustly simulated. Observed and simulated datasets were characterized by higher ET during most of dry season in the second ratoon cycle (300 DAR). This increased ET during this period is probably associated with higher levels of irrigation.

The dispersion diagram between observed and simulated results indicated that the model tended to underestimate ET in all range of ET values and for all experiments (Figure 23d). Experiment $1.00ET_0$ had the lowest bias (relative bias were -10.1%, -12.5%, and -12.1% for the $1.00ET_0$, $1.25ET_0$ and FRW, respectively), and the experiment $1.25ET_0$ presented the lowest correlation coefficient (for the $1.00ET_0$, $1.25ET_0$ and FRW experiments were 0.83, 0.85, and 0.84, respectively).

Simulated daily accumulation of above ground biomass (Figure 24) showed a classical s-shaped curve. Initial growth was more accurately simulated in the FRW experiment, with the $1.00ET_0$ and $1.25ET_0$ simulations showing higher errors. These errors were related to a strong photosynthesis reduction due to water shortage in simulations around DAR 127 (Note that model simulated less ET during this period – Figure 23a-b). Final values for observed/simulated biomass for the $1.00ET_0$, $1.25ET_0$, and FRW treatments were 5.69/4.87 $kg.m^{-2}$, 6.0/5.22 $kg.m^{-2}$, and 5.92/5.61 $kg.m^{-2}$ with a relative bias of -14.5%, -12.9%, and -5.3%, respectively. The simulations displayed wide deviations for the second ratoon cycle (Figure 24), in part due to the differences in LAI development in the first months after ratooning (see the Figure 22).

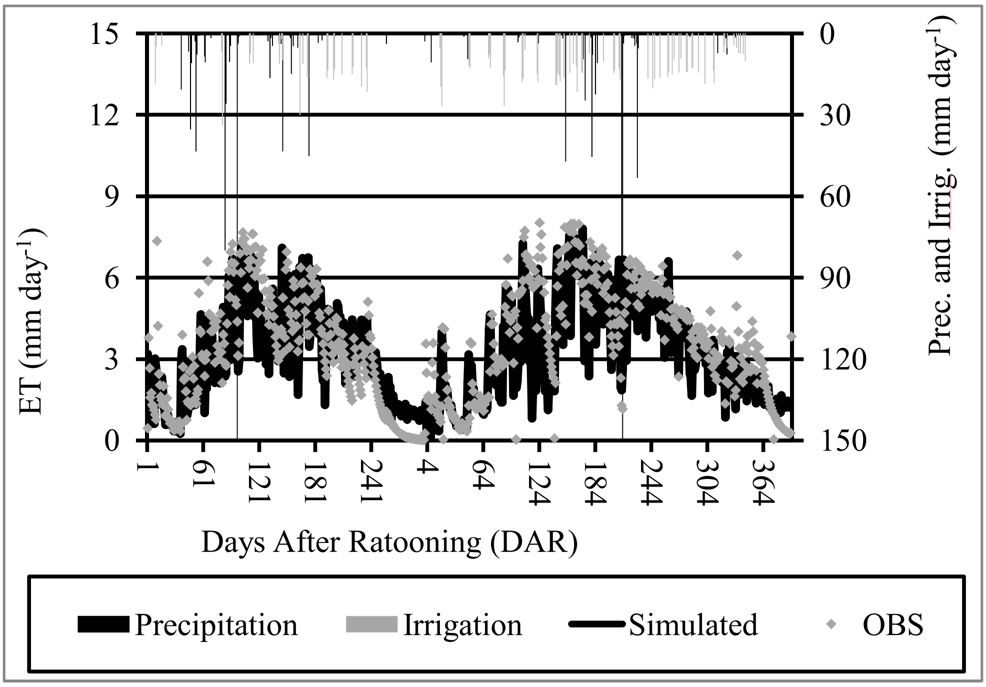
15
12
9
6
3
0
ET (mm day^{-1})
0
30
60
90
120
150
Prec. and Irrig. (mm day^{-1})
1
61
121
181
241
4
64
124
184
244
304
364
Days After Ratooning (DAR)
Precipitation
Irrigation
Simulated
OBS

(a)

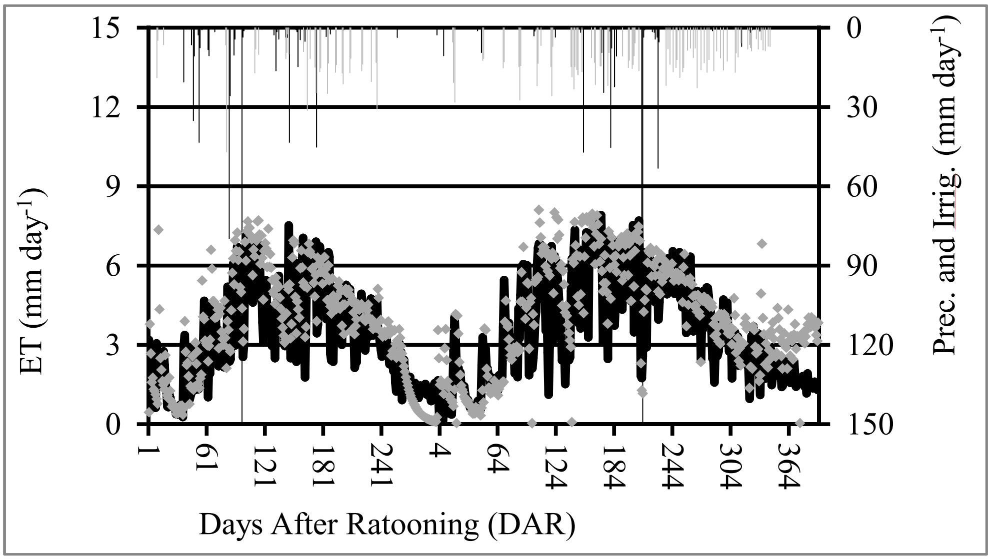
15
12
9
6
3
0
ET (mm day^{-1})
0
30
60
90
120
150
Prec. and Irrig. (mm day^{-1})
1
61
121
181
241
4
64
124
184
244
304
364
Days After Ratooning (DAR)

(b)

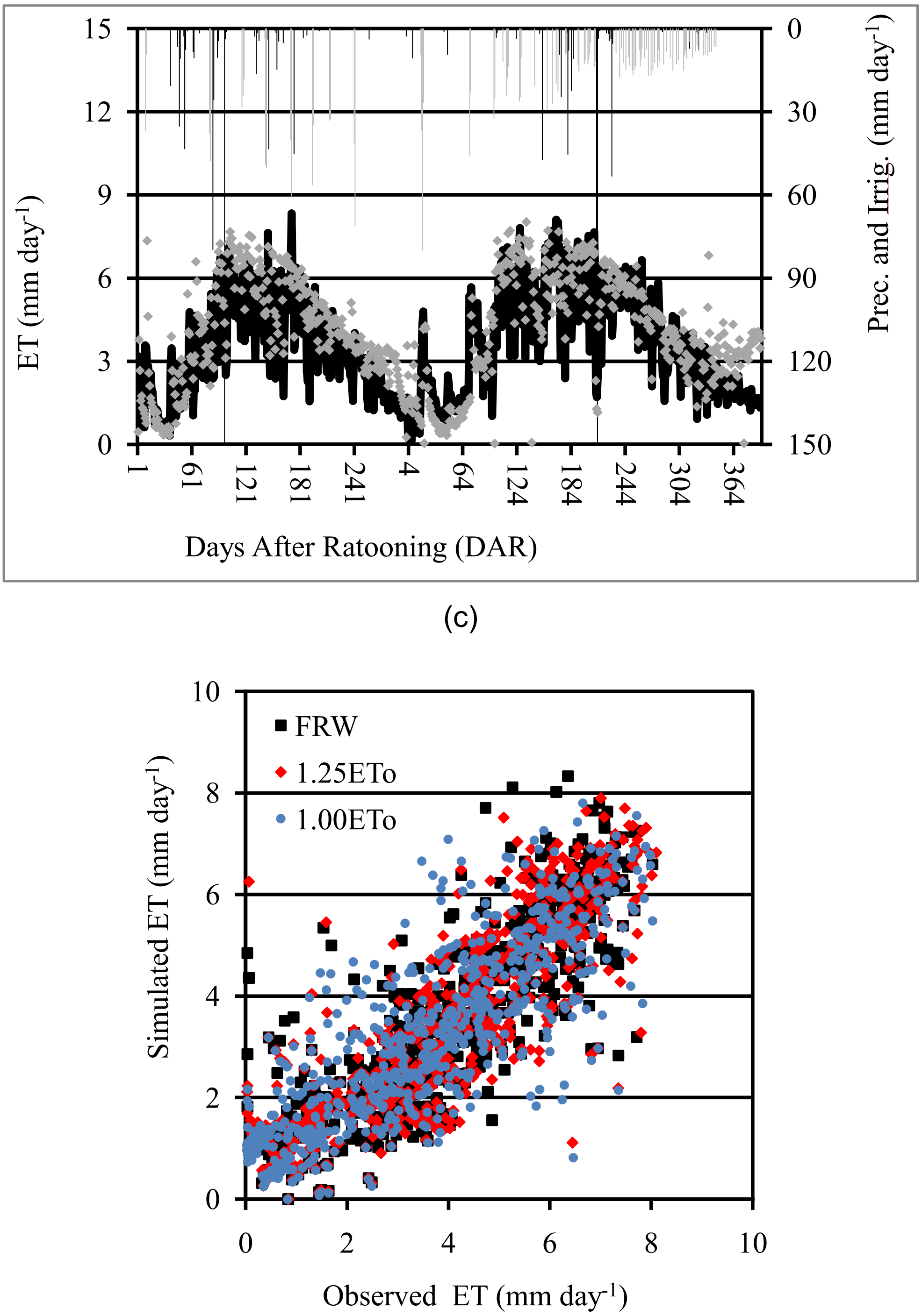

(c)

(d)

Figure 23 – Observed (gray symbol) and simulated (black line) daily evapotranspiration (ET – mm.day^{-1}) for the three different irrigation treatments (see text): (a) 1.0xET_0 irrigation; (b) 1.25xET_0 irrigation; and (c) Furrow irrigation. Precipitation (dark column) and Irrigation (gray column) are plotted in the right axis. (d) Dispersion diagram between observed and simulated daily ET: 1.0xET_0 irrigation (gray circles), 1.25xET_0 irrigation (red diamonds), and furrow irrigation (black squares).

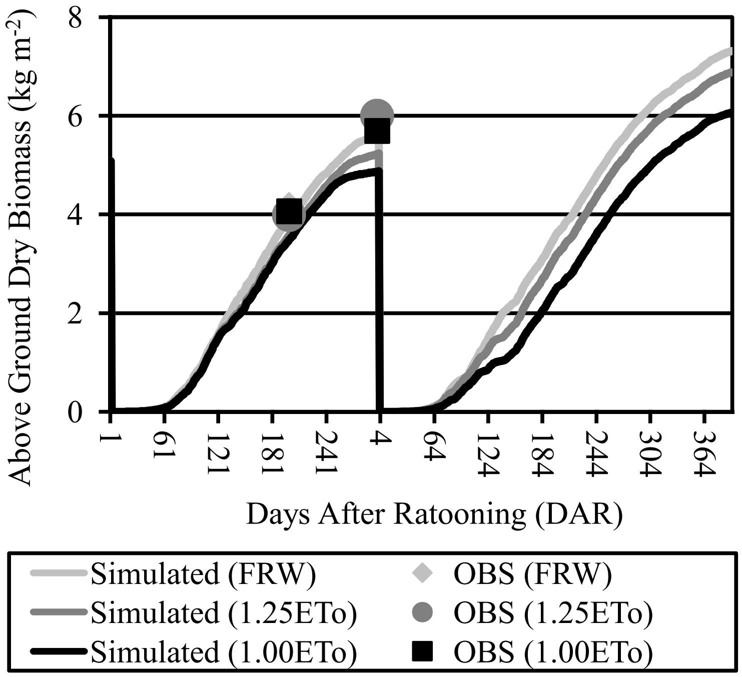

Figure 24 – Observed (symbols) and simulated (lines) above ground dry biomass (kg m^{-2}) over two consecutive ratoon cycles for the three irrigation treatments: 1.00 x ET0 (black); 1.25 x ET0 (dark gray); and furrow irrigation (light gray).

3.3. São Paulo mesoregions

Simulated average yield for the four São Paulo state mesoregions (Figure 25) were generally in good agreement with observed data, with a relative bias of less than 1.1%. Ribeirão Preto had the highest observed yield (79.4 $t.ha^{-1}$), followed by Bauru (77.9 $t.ha^{-1}$), São Jose do Rio Preto (76.9 $t.ha^{-1}$), and Araçatuba (75.9 $t.ha^{-1}$). The model accurately captured this spatial variability, simulating the highest yield for Ribeirão Preto (80.4 $t.ha^{-1}$), followed by Bauru (77.4 $t.ha^{-1}$), São Jose do Rio Preto (76.4 $t.ha^{-1}$) and Araçatuba (76.4 $t.ha^{-1}$).

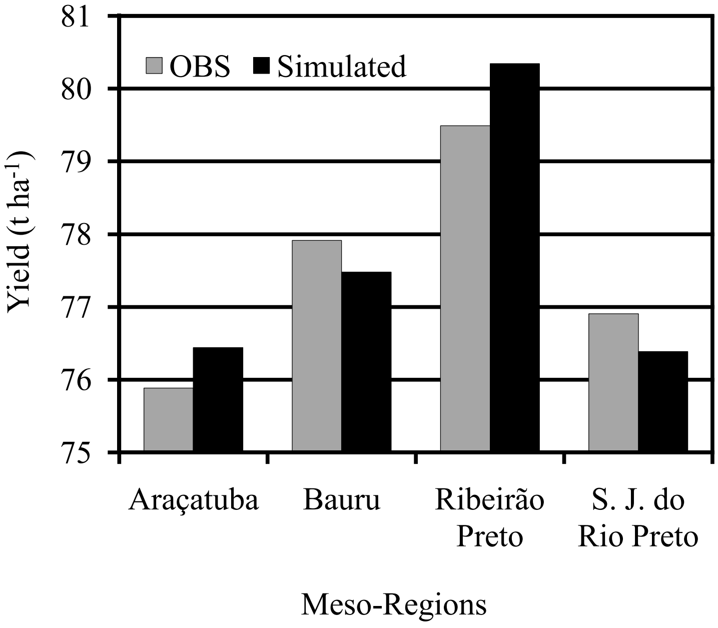

Figure 25 – Average (1990-2005) observed and modeled sugarcane yield (t·ha^{-1}) for the four mesoregions.

The pattern of dispersion between observed and simulated yield for all points (sixteen years and four mesoregions, Figure 26a) suggested that Agro-IBIS did not have any major systematic biases, and the points oscillated around the 1:1 line (RMSE = 3.6 t ha^{-1}). There were two outliers corresponding to yield underestimations in 2000 (Figures 27a and 27d), see in Figure 26c that model tended to overestimate the yield correlation with precipitation. Relative bias for all points was -0.15% with a correlation coefficient of 0.44.

The observed and modeled relationships between yield and growing season temperature (Figure 26b) were quite similar (giving almost identical quadratic regressions). Both regressions suggested a maximum yield for growing season temperature of around 23^{o}C. Yield is positively correlated with precipitation (Figure 26c), and the model overestimated the strength of this relationship. The observed linear regression suggests that yield increased 2.19 t·ha^{-1} for each mm day^{-1}, but the simulated response was 4.96 t·ha^{-1} for each mm day^{-1} (note that the range of precipitation variability varies from 2.5 to 5.0 mm day^{-1}, or 912 to 1825 mm year^{-1}).

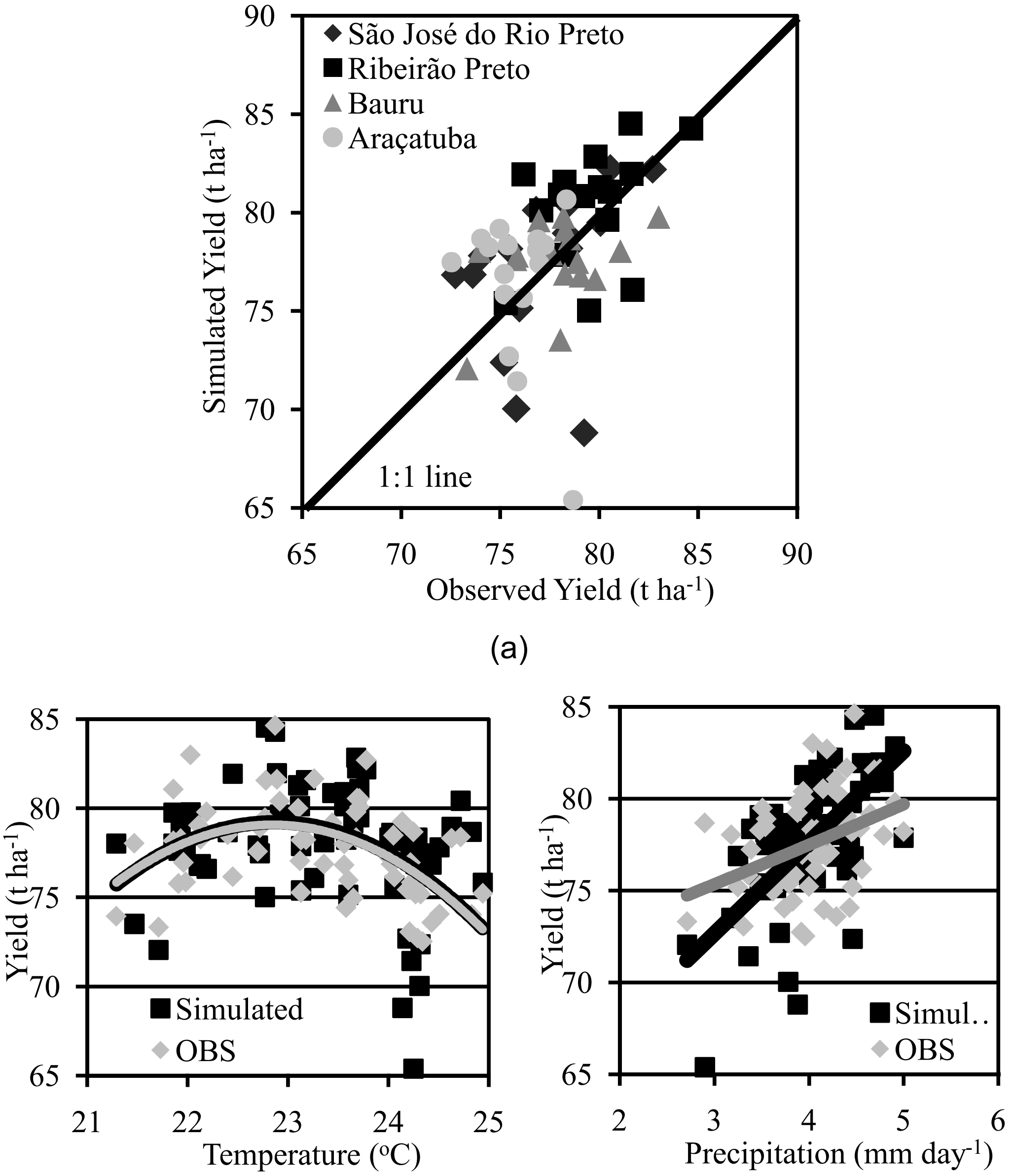

(a)

(b)

(c)

Figure 26 – Dispersion diagram between observed and simulated sugarcane yield for all years and mesoregions (black line shows the 1:1 relation) (a); observed (gray symbols) and modeled (black symbols) sugarcane yield (t ha^{-1}), considering all years and mesoregions, against growing season (b) temperature (^{o}C) and (c) precipitation (mm day^{-1}). In (b) and (c) lines display the linear regressions.

Considering the results from all regions, the model showed a similar average and amplitude of yield fluctuations compared with the observed data (Figure 27a-d). In Araçatuba (Figure 27a) modeled yield was negatively correlated (r = -0.28) with observed yield, although by excluding the data for the year 2000 the correlation increased to 0.16 and model's relative bias stayed low (from 0.73% to 1.7%). For the Bauru mesoregion (Figure 27b) simulated yield was similar to observed for most years (r = 0.41), and also produced a low relative bias (-0.56%). Interannual variability in yield for Ribeirão Preto (Figure 27c) follows the pattern observed in Bauru (Figure 27b), but with more pronounced oscillations. In Ribeirão Preto the model had a bias of 1.08% and correlation coefficient of 0.41. Finally, in São Jose do Rio Preto (Figure 27d), the observed and modeled data showed the highest interannual variability in yield. Relative bias was also low (-0.68%) and correlation with observed series was the highest (r = 0.50) among the simulations.

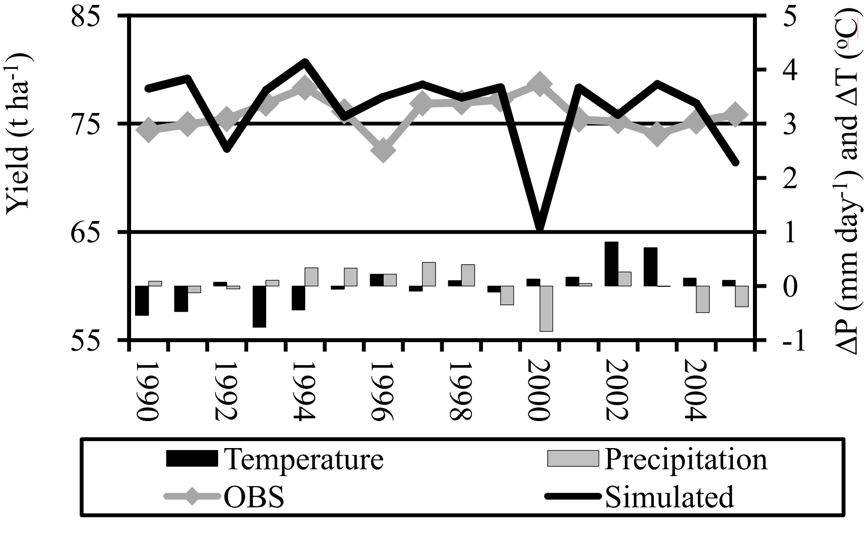

(a)

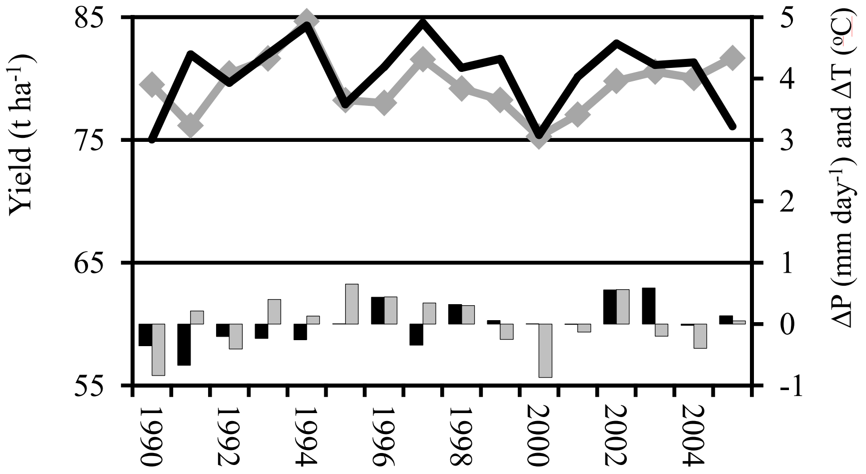
Yield (t ha^{-1})
ΔP (mm day^{-1}) and ΔT (°C)
85
75
65
55
5
4
3
2
1
0
-1
1990
1992
1994
1996
1998
2000
2002
2004

(b)

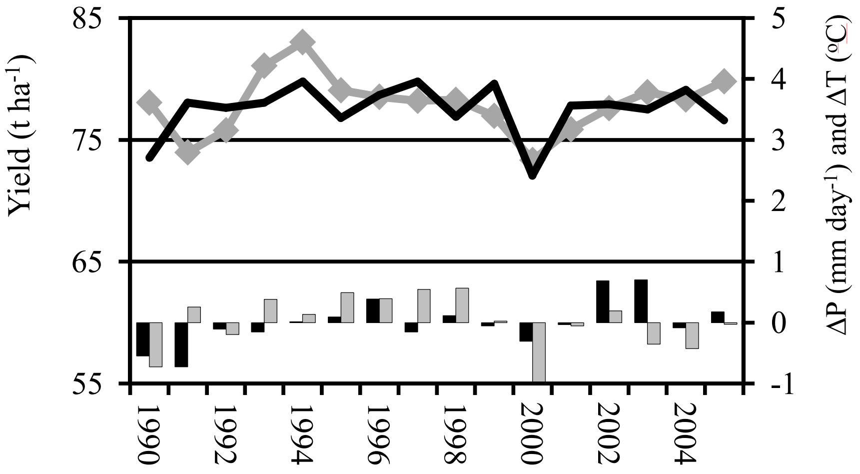
Yield (t ha^{-1})
ΔP (mm day^{-1}) and ΔT (°C)
85
75
65
55
5
4
3
2
1
0
-1
1990
1992
1994
1996
1998
2000
2002
2004

(c)

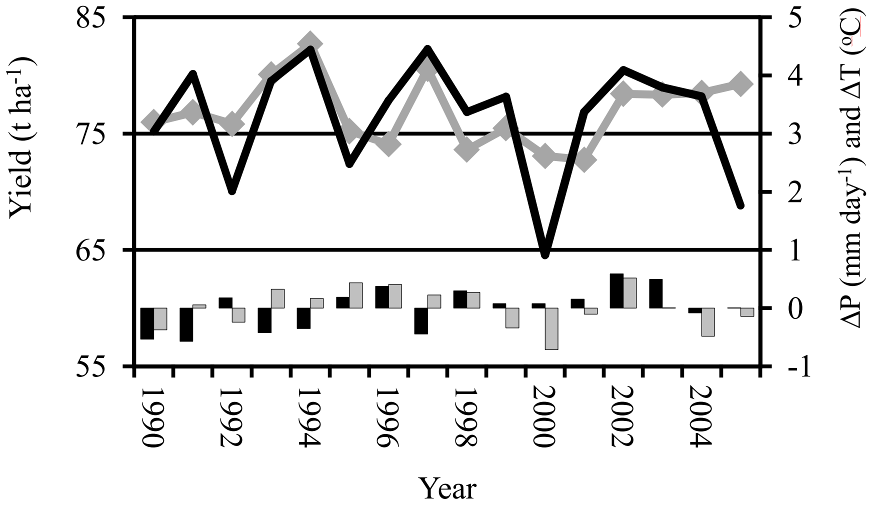

(d)

Figure 27 – Observed (Detrended – gray line) and modeled (black line) sugarcane yield (t ha^{-1}) for the mesoregions: (a) Araçatuba; (b) Bauru; (c) Ribeirão Preto; (d) São José do Rio Preto. Growing season temperature (^{o}C - black columns) and precipitation (mm day^{-1} – gray columns) anomalies are plotted on right axis.

3.4. Louisiana state

The modeled and (detrended) observed statewide yield data (1963 to 1993) from Louisiana were characterized by similar magnitude (relative bias equal to -2.67%), although the simulated quantities had a lower interannual variability (Figure 28). The correlation coefficient and RMSE between observed and modeled yield were equal to 0.26 and 4.83 t ha^{-1}, respectively.

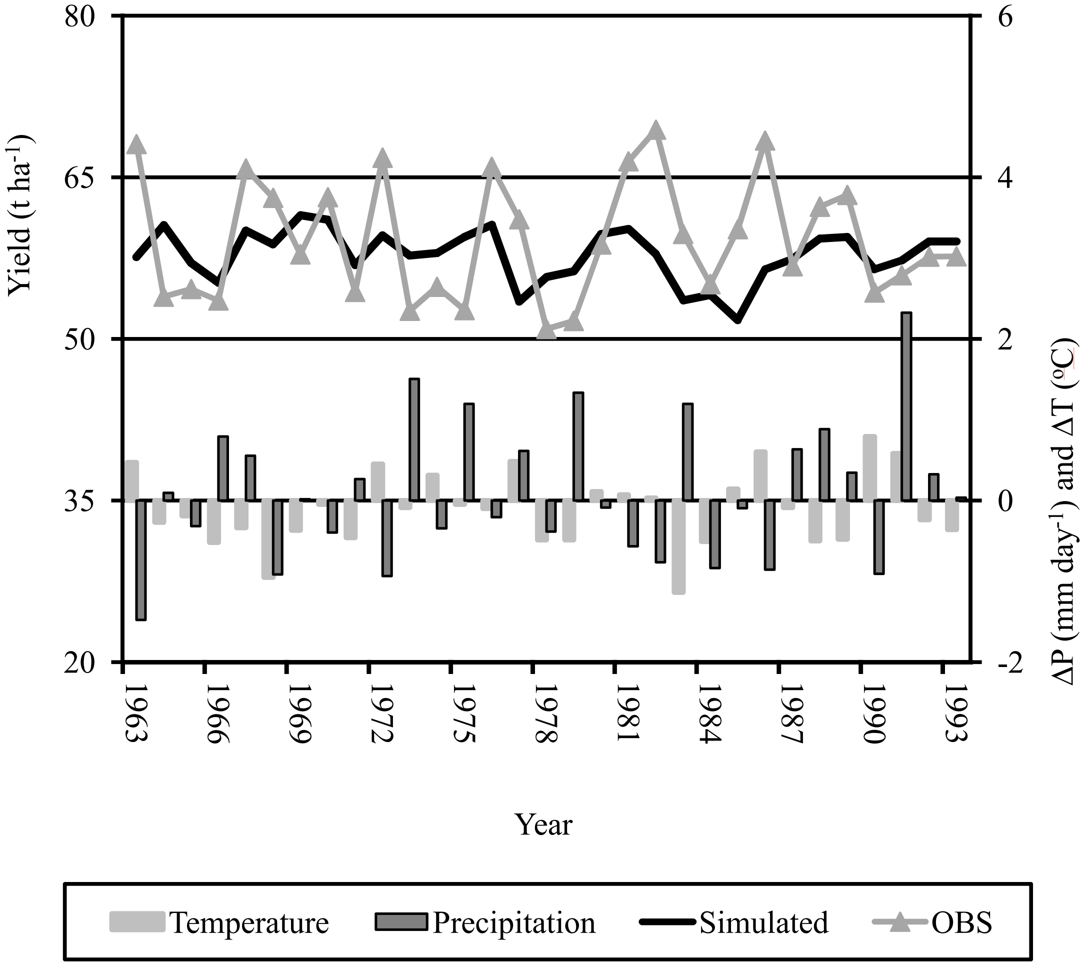

Figure 28 – Observed (detrended, gray line) and simulated (black line) average annual sugarcane yield for the Louisiana state. Growing season temperature (°C – light gray column) and precipitation (mm day^{-1} – dark gray column) anomalies are plotted in the right axis scale.

Yield had a positive relationship with winter temperature in both observed and simulated data (Figure 29a). To capture this positive relationship, the model considers that LAI is linearly reduced for temperature ranging from 0.0°C to -5.6°C, whereas at lower temperatures the sugarcane is assumed to die – see Part I for further details (CUADRA et al., submitted). The model was also able to accurately simulate the negative relationship between yield and winter precipitation (Figure 29b).

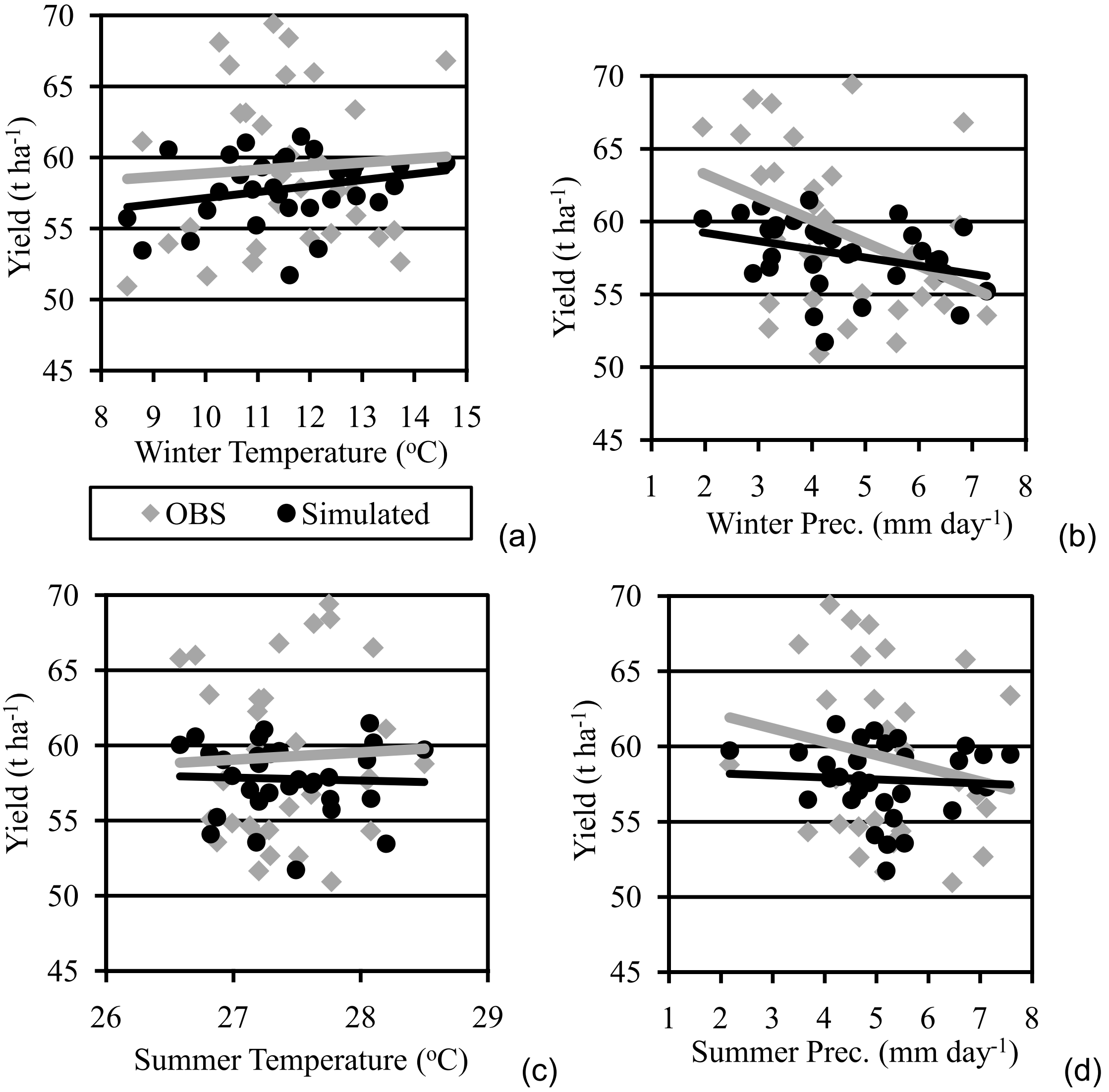

Figure 29 – Detrended observed (DT – gray symbols) and simulated (black symbols) dispersion diagram between sugarcane yield (t ha^{-1}) for the Louisiana state and: (a) average winter (January, February, and March) temperature; (b) average winter precipitation (same period); (c) average summer (July, August, and September) temperature; (d) average summer precipitation (same period).

Observed yield was weakly correlated with temperature and negatively correlated with precipitation over the summer (Figure 29c-d). In both cases the model failed to effectively capture these relationships. This failure was related to the strong negative correlation between summer precipitation and temperature. The model, by simulating a smaller negative correlation with precipitation, failed to capture both relationships (Figure 29c-d). Most of sugarcane cultivated in Louisiana has access to a water table and high precipitation amounts therefore tend to decrease yield (GREENLAND, 2005). Agro-IBIS would therefore need to include representation of groundwater to be able to more effectively capture these relationships and improve the model’s robustness over this region (and others where crops have access to an elevated water table).

3.5. Relative bias

For the São Paulo simulations (Figure 30), relative bias did not have any systematic relationship with precipitation or temperature, and the bias was relatively small (< 20%) across the range of temperature and precipitation (Figure 30a). By contrast, relative bias for the Louisiana simulations was clearly correlated with precipitation, overestimating the yield for high levels of precipitation and underestimating for low levels of precipitation (Figure 30b).

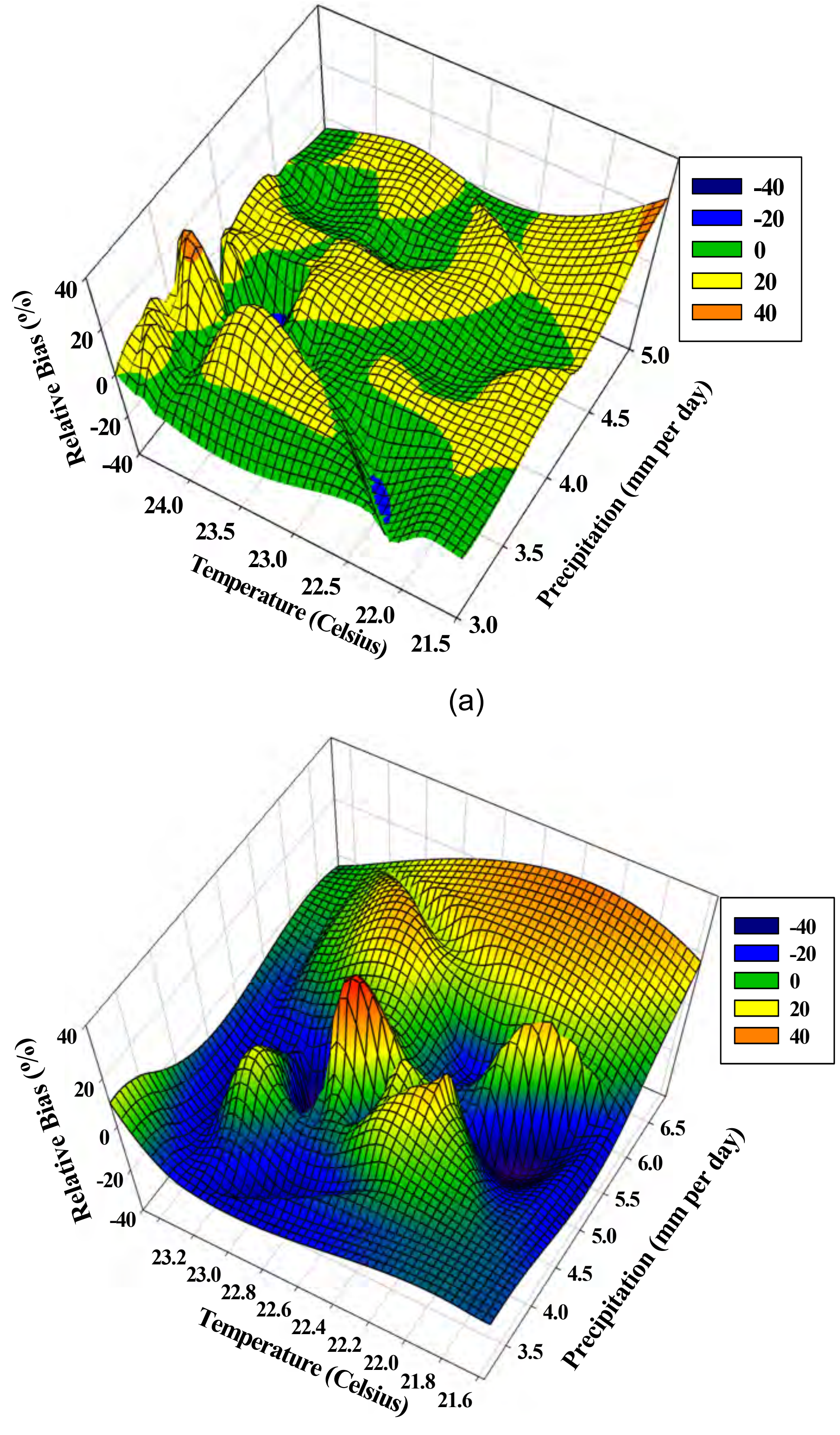

(a)

(b)

Figure 30 – Relative bias (% - z axis) versus growing season precipitation (mm day^{-1} – y axis) and temperature (^{o}C – x axis) – considering all mesoregions simulations (see Figure 2 for mesoregions names and locations) (a); same as (a) but for the Louisiana state simulation (b).

4. SUMMARY AND CONCLUSIONS

The new process-based sugarcane model has been developed to run as a module within the Agro-IBIS dynamic agro-ecosystem model. In addition to the assessment of climate change impacts on cropping systems, this modeling approach can capture the impact of land use on climate through simulation of the bi-directional feedbacks between the atmosphere and cropping systems.

Micrometeorological validation showed that through the inclusion of the new set of equations and parametrizations, the model accurately simulated the high frequency (hourly average) relationship between carbon assimilation and atmospheric conditions. The simulations illustrated low deviations of daily reflectances, resulting in a close approximation of daily solar radiation absorption. Net radiation partitioning (between latent and sensible heat fluxes) deviated from observations and the model systematically overestimated daily evapotranspiration when compared against the micrometeorological observations (Southeast Brazil), but underestimated ET when compared against the Australian field experiments, although these biases are probably within the uncertainty range of the observations. In both cases the model consistently reproduced daily variability. Future coupled simulations are being developed to investigate if the representation of crop cover (in regions under extensive agricultural cultivation) can improve weather and climate forecasts.

Considering all the validation simulations, the model was able to simulate accurately the average yield, but is less able to capture yield interannual variability. The relationship between yield and climate (temperature and precipitation) variability was accurately simulated for the São Paulo state (Brazil). In general, the model tended to overestimate the correlation between yield and precipitation, but with the correct signal. These results support the analyses presented in Part I, which demonstrated that the model consistently simulates the high frequency (hourly average) biophysical responses to atmospheric conditions. However, the relationship between yield and precipitation was overestimated for the Louisiana state (U.S.) simulation due to the lack of groundwater representation in the model.

Although this is the first version of this sugarcane module and some processes have not been incorporated (e.g. water table parametrization), the results of the validation indicate that this new module can be used to realistically simulate the sugarcane cropping system interactions with the atmosphere. Significantly, the future coupling of Agro-IBIS to a GCM will allow the bi-directional feedbacks between the atmosphere and cropping systems. Some important advantages of this approach include the improved evaluation of the impacts and interactions between crops and environmental parameters, as well as sensitivity experiments that explore the impacts of selected biophysical differences (between crops and the original biome; e.g., GEORGESCU et al., 2009) or the effective environmental benefits/harm of emerging bio-geoengineering under different regions and circumstances (e.g., MAKINO et al., 2000; SINGARAYER et al., 2007; SUZUKI et al., 2002).

Finally, it is important to note that the use of off-line simulations can also contribute to regional and local crop yield assessments under current conditions and climate change scenarios. Using this methodology, land use change impacts on environmental goods and services (e.g., biofuels, food, carbon sequestration, climate regulation), and related case studies and scenarios may be explored in further detail with Agro-IBIS.

REFERENCES

ALEXANDROV, V.A.; HOOGENBOOM, G. The impact of climate variability and change on crop yield in Bulgaria. **Agric. For. Meteorol.**, v. 104, p. 315-327, 2000.

BAIGORRIA, G.A.; JONES, J.W.; SHIN, D.W.; MISHRA, A.; O'BRIEN, J.J. Assessing uncertainties in crop model simulations using daily bias-corrected regional circulation model outputs. **Clim. Res.**, v. 34, p. 211-222, 2007.

BALL, J.T.; WOODROW, I.E.; BERRY, J.A. A model predicting stomatal conductance and its contribution to the control of photosynthesis under different environmental conditions. In: BIGGENS, J. (Ed.). **Progress in photosynthesis research**. Dordrecht: Martinus Nijhoff, 1987. v. 4, p. 221-224.

BETTS, R.A. Integrated approaches to climate-crop modelling: needs and challenges. **Phil. Trans. R. Soc. B.**, v. 360, p. 2049-2065, 2005.

BETTS, R.A.; FALLOON, P.D.; GOLDEWIJK, K.K.; RAMANKUTTY, N. Biogeophysical effects of land use on climate: model simulations of radiative forcing and large-scale temperature change. **Agric. Forest Meteorol.**, v. 142, p. 216-233, 2007.

BONDEAU, A.; SMITH, P.C.; ZAEHLE, S.; SCHAPHOFF, S.; LUCHT, W.; CRAMER, W.; GERTEN, D.; LOTZE-CAMPEN, H.; MULLER, C.; REICHSTEIN, M.; SMITH, B. Modelling the role of agriculture for the 20th century global terrestrial carbon balance. **Global Change Biol.**, v. 13, p. 679-706, 2007.

CHALLINOR, A.J.; WHEELER, T.R.; SLINGO, J.M.; CRAUFURD, P.Q.; GRIMES, D.I.F. Simulation of crop yields using the ERA40 re-analysis: limits to skill and non-stationarity in weather-yield relationships. **J. Appl. Meteorol.**, v. 44, p. 516-531, 2005.

COE, M.T.; COSTA, M.H.; SOARES-FILHO, B.S. The Influence of historical and potential future deforestation on the stream flow of the Amazon River – land surface processes and atmospheric feedbacks. **J. Hydrol.**, v. 369, p. 165-174, 2009.

COLLATZ, G.J.; RIBAS-CARBO, M.; BERRY, J.A. Coupled photosynthesis-stomatal conductance model for leaves of C4 plants. **Aust. J. Plant Physiol.**, v. 19, p. 519-538, 1992.

COSTA, M.H.; FOLEY, J.A. Combined effects of deforestation and doubled atmospheric CO_2 concentrations on the climate of Amazonia. **J. Climate**, v. 13, p. 18-34, 2000.

COSTA, M.H.; YANAGI, S.N.M. Effects of deforestation on the regional climate – historical perspectives, current and future research. **Rev. Bras. Meteorol.**, v. 21, p. 200-211, 2006.

COSTA, M.H.; YANAGI, S.N.M.; SOUZA, P.J.O.P.; RIBEIRO, A.; ROCHA, E.J.P. Climate change in Amazonia caused by soybean cropland expansion, as compared to caused by pastureland expansion. **Geophys. Res. Lett.**, v. 34, p. L07706, 2007.

CUADRA, S.V.; COSTA, M.H.; KUCHARIK, C.J.; DA ROCHA, R.P.; LEITE, C.C. A biophysical sugarcane growth model for global studies. Part II: Modeling Sugarcane agro-system Yield. **Agricultural and Forest Meteorology**, s.d. (Submitted).

DAI, A. Precipitation characteristics in eighteen coupled climate models. **J. Climate**, v. 19, p. 4605-4630, 2006.

DI VITTORIO, A.V.; ANDERSON, R.S.; WHITE, J.D.; MILLER, N.L.; RUNNING, S.W. Development and optimization of an Agro-BGC ecosystem model for C4 perennial grasses. **Ecol. Model.**, doi:10.1016/j.ecolmodel.2010.05.013, 2010.

DUBROVSKY, M.; ZALUD, Z.; STASTNA, M. Sensitivity of ceres-maize yields to statistical structure of daily weather series. **Clim. Change**, v. 46, p. 447-472, 2000a.

DUBROVSKY, M.; ZALUD, Z.; STASTNA, M.; TRNKA, M. Effect of climate change and climate variability on crop yields. In: EUROPEAN CONFERENCE ON APPLIED CLIMATOLOGY, 3, 2000, Pisa. **Proceedings…** Pisa, Italy, 2000b.

EASTERLING, W.E.; AGGARWAL, P.K.; BATIMA, P.; BRANDER, K.M.; ERDA, L.; HOWDEN, S.M.; KIRILENKO, A.; MORTON, J.; SOUSSANA, J.F.; SCHMIDHUBER, J.; TUBIELLO, F.N. Food, fibre and forest products. In: PARRY, M.L.; CANZIANI, O.F.; PALUTIKOF, J.P.; VAN DER LINDEN, P.J.; HANSON, C.E. (Eds.). **Climate change 2007**: impacts adaptation and vulnerability contribution of working group II to the Fourth Assessment Report of the Intergovernmental Panel on Climate Change. Cambridge, Cambridge University Press, 2007. p. 273-313.

EDMÉ, S.J.; MILLER, J.D.; GLAZ, B.; TAI, P.Y.P.; COMSTOCK, J.C. Genetic Contribution to yield gains in the Florida sugarcane industry across 33 years. **Crop Sci.**, v. 45, p. 92-97, 2005.

EMPRESA DE PESQUISA ENERGÉTICA – EPE. **Decadal energy expansion plane for 2008/2017**. Rio de Janeiro, 2009.

FARGIONE, J.; HILL, J.; TILMAN, D.; POLASKY, S.; HAWTHORNE, P. Land clearing and the biofuel carbon debt . **Science**, v. 319, p. 1235, 2008.

FARQUHAR, G.D.; VON CAEMMERER, S.; BERRY, J.A. A biochemical model of photosynthetic CO_2 assimilation in leaves of C3 species. **Planta**, v. 149, p. 78-90, 1980.

FEDDEMA, J.J.; OLESON, K.W.; BONAN, G.B.; MEARNS, L.O.; BUJA, L.E.; MEEHL, G.A.; WASHINGTON, W.M. The importance of land-cover change in simulating future. **Clim. Science**, v. 310, p. 1674-1678, 2005.

FELKNER, J.; TAZHIBAYEVA, K.; TOWNSEND, R. Impact of climate change on rice production in Thailand. **Amer. Econ. Rev.**, v. 99, p. 205-210, 2009.

FOLEY, J.A.; PRENTICE, I.C.; RAMANKUTTY, N.; LEVIS, S.; POLLARD, D.; SITCH, S.; HAXELTINE, A. An integrated biosphere model of land surface processes, terrestrial carbon balance, and vegetation dynamics. **Global Biogeochem. Cycles**, v. 10, n. 4, p. 603-628, 1996.

FOOD AND AGRICULTURE ORGANIZATION OF THE UNITED NATIONS – FAO. **The state of food and agriculture**. 2008. 138 p. (Technical report).

FORSTER, P.; RAMASWAMY, V.; ARTAXO, P.; BERNTSEN, T.; BETTS, R.; FAHEY, D.W.; HAYWOOD, J.; LEAN, J.; LOWE, D.C.; MYHRE, G.; NGANGA, J.; PRINN, R.; RAGA, G.; SCHULZ, M.; VAN DORLAND, R. Changes in atmospheric constituents and in radiative forcing. In: SOLOMON, S.; QIN, D.; MANNING, M.; CHEN, Z.; MARQUIS, M.; AVERYT, K.B.; TIGNOR, M.; MILLER, H.L. (Eds.). **Climate change 2007**: the physical science basis. Contribution of Working Group I to the Fourth Assessment Report of the Intergovernmental Panel on Climate Change. Cambridge: Cambridge University Press, 2007.

GEORGESCU, M.; LOBELL, D.B.; FIELD, C.B. Potential impact of U.S. biofuels on regional climate. **Geophys. Res. Lett.**, v. 36, p. L21806, 2009.

GERVOIS, S.; DE NOBLET-DUCOUDRÉ, N.; VIOVY, N.; CIAIS, P.; BRISSON, N.; SEGUIN, B.; PERRIER, A. Including croplands in a global biosphere model: methodology and evaluation at specific sites. **Earth Interact.**, v. 8, p. 1-25, 2004.

GIBBS, H.K.; JOHNSTON, M.; FOLEY, J.A.; HOLLOWAY, T.; MONFREDA, C.; RAMANKUTTY, N.; ZAKS, D. Carbon payback times for crop-based biofuel expansion in the tropics: the effects of changing yield and technology. **Environ. Res. Lett.**, v. 3, p. 034001, 2008.

GREENLAND, D. Climate variability and sugarcane yield in Louisiana. **J. Appl. Meteor.**, v. 44, p. 1655-1666, 2005.

HAIM, D.; SHECHTER, M.; BERLINER, P. Assessing the impact of climate change on representative field crops in Israeli agriculture: a case study of wheat and cotton. **Clim. Change**, v. 86, p. 425-440, 2008.

HOUGHTON, R.A. Balancing the global carbon budget. **Annu. Rev. Earth Pl. Sc.**, v. 35, p. 313-347, 2007.

HOUGHTON, R.A.; HACKLER, J.L. Carbon flux to the atmosphere from land-use changes. In: OAK RIDGE NATIONAL LABORATORY. Carbon Dioxide Information Analysis Center. **Trends: a compendium of data on global change**. Oak Ridge, Tenn., 2002.

INMAN-BAMBERA, N.G.; MUCHOWB, R.C.; ROBERTSON, M.J. Dry matter partitioning of sugarcane in Australia and South Africa. **Field Crops Res.**, v. 76, p. 71-84, 2002.

INTERNATIONAL ENERGY AGENCY – IEA. **World energy outlook 2006**. 2007. 599 p.

JUÁREZ, R.I.N.; HODNETT, M.G.; FU, R.; GOULDEN, M.L.; VON RANDOW, C. Control of dry season evapotranspiration over the amazonian forest as inferred from observations at a Southern Amazon Forest Site. **J. Climate**, v. 20, 2827-2839, 2007.

KEATING, B.A.; ROBERSTON, M.J.; MUCHOW, R.C.; HUTH, N.I. Modelling sugarcane production systems. I. Development and performance of the sugarcane module. **Field Crops Res.**, v. 61, p. 253-271, 1999.

KOTHAVALA, Z.; ARAIN, M.A.; BLACK, T.A.; VERSEGHY, D. The simulation of energy, water vapor and carbon dioxide fluxes over common crops by the Canadian Land Surface Scheme (CLASS). **Agr. Forest Meteorol.**, v. 133, p. 89-108, 2005.

KUCHARIK, C.J. Evaluation of a process-based agro-ecosystem model (Agro-IBIS) across the U.S. cornbelt: simulations of the inter-annual variability in maize yield. **Earth Interact.**, v. 7, p. 1-33, 2003.

KUCHARIK, C.J.; BRYE, K.R. Integrated biosphere simulator (IBIS) yield and nitrate loss predictions for Wisconsin maize receiving varied amounts of Nitrogen fertilizer. **J. Environ. Qual.**, v. 32, p. 247-268, 2003.

KUCHARIK, C.J.; FOLEY, J.A.; DELIRE, C.; FISHER, V.A.; COE, M.T.; LENTERS, J.D.; YOUNG-MOLLING, C.; RAMANKUTTY, N.; NORMAN, J.M.; GOWER, S.T. Testing the performance of a dynamic global ecosystem model: water balance, carbon balance, and vegetation structure. **Global Biogeochem. Cycles**, v. 14, n. 3, p. 795-825, 2000.

KUCHARIK, C.J.; TWINE, T.E. Residue, respiration, and residuals: evaluation of a dynamic agroecosystem model using eddy flux measurements and biometric data. **Agr. Forest Meteorol.**, v. 146, p. 134-158, 2007.

LI, W.; DICKINSON, R.E.; FU, R.; NIU, G.; YANG, Z.; CANADELL, J.G. Future precipitation changes and their implications for tropical peatlands. **Geophy. Res. Lett.**, v. 34, p. L01403, 2007.

LINN, D.M.; DORAN, J.W. Effect of water-filled pore space on carbon dioxide and nitrous oxide production in tilled and nontilled soils. **Soil Sci. Soc. Am. J.**, v. 48, p. 1267-1272, 1984.

LIU, D.L.; HELYAR, K.R. Simulation of seasonal stalk water content and fresh weight yield of sugarcane. **Field Crops Res.**, v. 82, p. 59-73, 2003.

LLOYD, J.; TAYLOR, J.A. On the temperature dependence of soil respiration. **Funct. Ecol.**, v. 8, p. 315-323, 1994.

LOKUPITIYA, E.; DENNING, S.; PAUSTIAN, K.; BAKER, I.; SCHAEFER, K.; VERMA, S.; MEYERS, T.; BERNACCHI, C.J.; SUYKER, A.; FISCHER, M. Incorporation of crop phenology in Simple Biosphere Model (SiBcrop) to improve land-atmosphere carbon exchanges from croplands. **Biogeosciences**, v. 6, p. 969-986, 2009.

MACEDO, I.C. **Feasibility of biomass-derived ethanol as a fuel for transportation**. (Project ME-T1007 - ATN/DO-9375-ME), activity 6: potentials in relation to sustainability criteria. México: SENER/BID, 2006.

MAKINO, A.; NAKANO, H.; MAE, T.; SHIMADA, T.; YAMAMOTO, N. Photosynthesis, plant growth and N allocation in transgenic rice plants with decreased Rubisco under CO_2 enrichment. **J. Exp. Bot.**, v. 51, p. 383-389, 2000.

MARLAND, G.; BODEN, T.A.; ANDRES, R.J. Global, regional, and national CO_2 emissions. In: OAK RIDGE NATIONAL LABORATORY. Carbon Dioxide Information Analysis Center. **Trends**: a compendium of data on global change. Oak Ridge, Tenn., 2007.

MEARNS, L.O.; EASTERLING, W.; HAYS, C.; MARX, D. Comparison of agricultural impacts of climate change calculated from high and low resolution climate change scenarios: Part I. The uncertainty due to spatial scale. **Clim. Change**, v. 51, p. 131-172, 2001.

MEEHL, G.A.; STOCKER, T.F.; COLLINS, W.D.; FRIEDLINGSTEIN, P.; GAYE, A.T.; GREGORY, J.M.; KITOH, A.; KNUTTI, R.; MURPHY, J.M.; NODA, A.; RAPER, S.C.B.; WATTERSON, I.G.; WEAVER, A.J.; ZHAO, Z.C. Global climate projections. In: SOLOMON, S.; QIN, D.; MANNING, M.; CHEN, Z.; MARQUIS, M.; AVERYT, K.B.; TIGNOR, M.; MILLER, H.L. (Eds.). **Climate change 2007**: the physical science basis. Contribution of Working Group I to the Fourth Assessment Report of the Intergovernmental Panel on Climate Change. Cambridge: Cambridge University Press, 2007.

MEINZER, F.C.; GRANTZ, D.A. Stomatal and hydraulic conductance in growing sugarcane: stomatal adjustment to water transport capacity. **Plant Cell Environ.**, v. 13, p. 383-388, 1990.

MILES, L.; GRAINGER, A.; PHILLIPS, O. The impact of global climate change on tropical forest biodiversity in Amazonia. **Global Ecol. Biogeogr.**, v. 13, p. 553-565, 2004.

MITCHELL, T.; JONES, P. An improved method of constructing a database of monthly climate observations and associated high-resolution grids. **Int. J. Climatol.**, v. 25, p. 693-712, 2005.

MUCHOW, R.C.; HUGHES, R.M.; HORAN, H.L. **Evaluating the potential for improved sugar yields by assessing the climatic and soil constraints to production in southern cane-growing districts**. 1999. 66 p. (Technical report).

NOBRE, C.A.; SELLERS, P.E.; SHUKLA, J., Amazonian deforestation and tropical climate. **J. Climate**, v. 19, p. 957-988, 1991.

OLESON, K.W. et al. CLM3.5 documentation, **Natl. Cent. for Atmos. Res.**, Boulder, 2007. (Technical report). Available at: <http://www.cgd.ucar.edu/tss/clm/distribution/ clm3.5/>.

ORGANIZATION FOR ECONOMIC CO-OPERATION AND DEVELOPMENT, FOOD AND AGRICULTURE ORGANIZATION OF THE UNITED NATIONS (OECD-FAO). **Agricultural Outlook 2007-2016**. 2007. 88 p. (Technical report).

ORGANIZATION FOR ECONOMIC CO-OPERATION AND DEVELOPMENT, FOOD/AGRICULTURE ORGANIZATION OF THE UNITED NATIONS – OECD-FAO. **The state of food and agriculture – Biofuels**: prospects, risk, and opportunities. 2008. 138 p. (Technical report).

OSBORNE, T.M.; LAWRENCE, D.M.; CHALLINOR, A.J.; SLINGO, J.M.; WHEELER, T.R. Development and assessment of a coupled crop-climate model. **Global Change Biol.**, v. 13, p. 169-183, 2007.

PARK, S.E.; ROBERTSON, M.J.; INMAN-BAMBER, N.G. Decline in the growth of a sugarcane crop with age under high input conditions. **Field Crops Res.**, v. 92, p. 305-320, 2005.

PARTON, W.J.; SCHIMEL, D.S.; COLE, C.V.; OJIMA, D.S. Analysis of factors controlling soil organic matter levels in great plains grasslands. **Soil Sci. Soc. Am. J.**, v. 51, p. 1173-1179, 1987.

PELLEGRINO, G.Q. **NOAA14/AVHRR spectral data as data source for fitomass models**. Campinas: FEAGRI-UNICAMP, 2001. 133 p. (in Portuguese).

PIELKE, R.A.; AVISSAR, R.; RAUPACH, M.; DOLMAN, A.J.; ZENG, X.; DENNING, A.S. Interactions between the atmosphere and terrestrial ecosystems: influence on weather and climate. **Global Change Biol.**, v. 4, p. 461-475, 1998.

PINTO, L.F.G.; BERNARDES, M.S.; PEREIRA, A.R.; Yield and performance of sugarcane in on-farm interface with rubber in Brazil. **Pesq. Agropec. Bras.**, v. 41, p. 251-255, 2006.

PRENTICE, I.C.; FARQUHAR, G.D.; FASHAM, M.J.R.; GOULDEN, M.L.; HEIMANN, M. et al. The carbon cycle and atmospheric carbon dioxide. In: HOUGHTON, J.T.; DING, Y.; GRIGGS, D.J.; NOGUER, M.; VAN DER LINDEN, PJ.; DAI, X.; MASKELL, K.; JOHNSON, C.A. **Climate change 2001**: the scientific basis. Contribution of Working Group I to the Third Assessment Report of the Intergovernmental Panel on Climate Change. Cambridge: Cambridge University Press, 2001. p. 239-287.

RADDATZ, R.L. Evidence for the influence of agriculture on weather and climate through the transformation and management of vegetation: illustrated by examples from the Canadian Prairies. **Agric. For. Meteorol.**, v. 142, p. 186-202, 2007.

RAJAGOPAL, D.; SEXTON, S.E.; ROLAND-HOLST, D.; ZILBERMAN, D. Challenge of biofuels: filling the tank without emptying the stomach? **Envir. Res. Lett.**, v. 2, p. 1-9, 2007.

RAMANKUTTY, N.; EVAN, A.T.; MONFREDA, C.; FOLEY, J.A. Farming the planet. Part 1: The geographic distribution of global agricultural lands in the year 2000. **Global Biogeochem. Cycles**, v. 22, p. GB1003, 2008.

RANDALL, D.A.; WOOD, R.A.; BONY, S.; COLMAN, R.; FICHEFET, T.; FYFE, J.; KATTSOV, V.; PITMAN, A.; SHUKLA, J.; SRINIVASAN, J.; STOUFFER, R.J.; SUMI, A.; TAYLOR, K.E. Climate models and their evaluation. In: SOLOMON, S.; QIN, D.; MANNING, M.; CHEN, Z.; MARQUIS, M.; AVERYT, K.B.; TIGNOR, M.; MILLER, H.L. (Eds.). **Climate change 2007**: the physical science basis. Contribution of Working Group I to the Fourth Assessment Report of the Intergovernmental Panel on Climate Change. Cambridge: Cambridge University Press, 2007.

RAUPACH, M.R.; MARLAND, G.; CIAIS, P.; LE QUÉRÉ, C.; CANADELL, J.G.; KLEPPER, G.; FIELD, C.B. Global and regional drivers of accelerating CO_2 emissions. **PNAS**, v. 104, p. 10288-10293, 2007

RICHARDSON, C.W.; WRIGHT, D.A. **WGEN**: A model for generating daily weather variables. Washington, D.C.: USDA, 1984.

RÍPOLI, T.C.C.; MOLINA, W.F.; RIPOLI, M.L.C. Energy potential of sugar cane biomass in Brazil. **Scientia Agricola**, v. 57, p. 677-681, 2002.

ROBERTSON, M.J.; WOOD, A.W.; MUCHOW, R.C. Growth of sugarcane under high input conditions in tropical Australia. I. Radiation use, biomass accumulation and partitioning. **Field Crops Res.**, v. 48, p. 11-25, 1996.

SACKS, W.J.; DERYNG, D.; FOLEY, J.A.; RAMANKUTTY, N. Crop planting dates: an analysis of global patterns. **Global Ecology and Biogeography**, doi:10.1111/j.1466-8238.2010.00551.x, 2010.

SCHOLZE, M.; KNORR, W.; ARNELL, N.W.; PRENTICE, I.C. A climate-change risk analysis for world ecosystems. **PNAS**, v. 103, p. 13116-13120, 2006.

SHIN, D.W.; BAIGORRIA, G.A.; LIM, Y.K.; COCKE, S.; LAROW, T.E.; O'BRIEN, J.J.; JONES, J.W. Assessing crop yield simulations with various seasonal climate data. **Science and Technology Infusion Climate Bulletin**, Norman, OK, p. 24-27, 2009.

SINGARAYER, J.S.; RIDGWELL, A.; IRVINE, P. Assessing the benefits of crop albedo bio-geoengineering. **Environ. Res. Lett.**, v. 4, p. 045110, 2009.

SINGELS, A.; BEZUIDENHOUT, C.N. A new method of simulating dry matter partitioning in the Canegro sugarcane model. **Field Crop Res.**, v. 78, p. 151-164, 2002.

SINGELS, A.; DONALDSON, R.A.; SMIT, M.A. Improving biomass production and partitioning in sugarcane: theory and practice. **Field Crops Res.**, v. 92, p. 291-303, 2005.

SMITH, D.M.; INMAN-BAMBER, N.G.; THORBURN, P.J. Growth and function of the sugarcane root system. **Field Crops Res.**, v. 92, p. 169-183, 2005.

SMITH, M.A.; SINGELS, A. The response of sugarcane canopy development to water stress. **Field Crops Res.**, v. 98, p. 91-97, 2006.

SNYDER, P.K.; FOLEY, J.A. Analyzing the effects of complete tropical forest removal on the regional climate using a detailed three-dimensional energy budget: an application to Africa. **J. Geophy. Res.**, v. 109, p. D21102, 2004.

SOUZA, Z.M.; PRADO, R.M.; PAIXÃO, A.C.S.; CESARIN, L.G. Harvest systems and residue management of sugarcane. **Pesq. Agropec. Bras.**, v. 40, p. 271-278. 2005. (in Portuguese).

SOUZA-FILHO, J.D.C.; RIBEIRO, A.; COSTA, M.H.; COHEN, J.C.P. Mecanismos de controle da variação sazonal da transpiração de uma floresta tropical no nordeste da Amazônia. **Acta Amazonica**, v. 35, p. 235-241, 2005.

SUZUKI, S. ; MURAI, N. ; BURNELL, J.N. ; ARAI, M. C4 photosynthesis: principles of CO_2 concentration and prospects for its introduction into C3 plants. **J. Exp. Bot.**, v. 53, p. 581-590, 2002.

TATSCH, J.D.; BINDI, M.; MORIONDO, M. A preliminary evaluation of the cropsyst model for sugarcane in the Southeast of Brazil. In: BINDI. M.; BRANDANI, G.; DIBARI, C.; DESSÌ, A.; FERRISE, R.; MORIONDO, M.; TROMBI, G. (Orgs.). **Impact of climate change on agricultural and natural ecosystems**. Florença, Itália: Firenze University Press, 2009. p. 75-84.

THOMPSON, G.D. Production of biomass by sugarcane. **Proc. S. Afr. Sugar Technol. Assoc.**, v. 52, p. 180-187, 1978.

TSVETSINSKAYA, E.A.; MEARNS, L.O.; EASTERLING, W.E. Investigating the effect of seasonal plant growth and development in three-dimensional atmospheric simulations. Part I: Simulation of surface fluxes over the growing season. **J. Clim.**, v. 14, p. 692-709, 2001.

TUBIELLO, F.N.; SOUSSANA, J.F.; HOWDEN, S.M. Crop and pasture response to climate change. **PNAS**, v. 104, p. 19686-19690, 2007.

TWINE, T.E.; KUCHARIK, C.J.; FOLEY, J.A. Effects of land cover change on the energy and water balance of the Mississippi river basin. **J. Hydrometeorol.**, v. 5, p. 640-655, 2004.

VERBERNE, E.L.J.; HASSINK, J.; DE WILLIGEN, P.; GROOT, J.J.R.; VAN VEEN, J.A. Modelling organic matter dynamics in different soils. **Neth J. Agric. Sci.**, v. 38, p. 221-238, 1990.

WANG, G. Agricultural drought in a future climate: results from 15 global climate models participating in the IPCC 4th assessment. **Clim. Dyn.**, v. 25, p. 739-753, 2005.